ACS APPLIED MATERIALS & INTERFACES

Review

www.acsami.org

Bioinspired Wetting Surface via Laser Microfabrication

Feng Chen,* Dongshi Zhang, Qing Yang, Jiale Yong, Guangqing Du, Jinhai Si, Feng Yun, and Xun Hou

State Key Laboratory for Manufacturing Systems Engineering & Key Laboratory of Photonics Technology for Information of Shaanxi Province, School of Electronics & Information Engineering, Xi'an Jiaotong University, Xi'an 710049, China

ABSTRACT: Bioinspired special wettibilities including superhydrophobicity and tunable adhesive force have drawn considerable attention because of their significant potential for fundamental research and practical applications. This review summarizes recent progress in the development of bioinspired wetting surfaces via laser microfabrication, with a focus on controllable, biomimetic, and switchable wetting surfaces, as well as their applications in biology, microfluidic, and paper-based devices, all of which demonstrate the ability of laser microfabrication in producing various multiscale structures and its adaptation in a great variety of materials. In particular, compared to other techniques, laser microfabrication can realize special modulation ranging from superhydrophilic to superhydrophobic without the assistance of fluorination, allowing much more freedom to achieve complex multiple-wettability integration. The current challenges and future research prospects of this rapidly developing field are also being discussed. These approaches open the intriguing possibility of the development of advanced interfaces equipped with the integration of more functionalities.

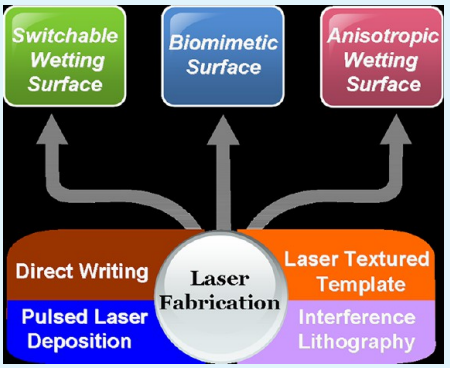

KEYWORDS: *bioinspired surface, biomemetic surface, laser microfabrication, hierarchical structures, switchable wetting surface*

1. INTRODUCTION

After billions of years of evolution on this planet, biological surfaces exhibit almost perfect multifunctional interfaces to adjust to harsh environment.[1] Among all of the functional properties of natural surfaces, a large diversity of wettabilities have gained more and more attention recently because of their potentially wide range of applications in people's daily life and industrial fields,[2,3] such as anticorrosion, anti-icing, and low hydrodynamic friction, thus revealing a cornucopia of functional wetting surfaces.[4,5] For example, lotus leaf exhibits superhydrophobicity and self-cleaning ability, which enable a water drop to easily move off the surface and take away the adhesive debris.[6] The floating water fern Salvinia[7] (Figure 1a–d) and Mosquito compound eye[8] (Figure 1m,n) have the ability of long-term air retention and antifogging, respectively. The wing of a Morpho aega butterfly[9] (Figure 1e) exhibits directionally adhesive wettability, where a droplet can easily roll off along the radial-outward (RO) direction of the central axis of the butterfly's body but pin tightly against the RO direction. A tokay gecko[10] (Figure 1f–j) can virtually cling to any surface and support its body mass with a single toe by using millions of keratinous setae on its toe pads. Some beetles[11] in the Namib Desert can collect drinking water from fog-laden wind on their bumpy surface (Figure 1k,l) consisting of alternating hydrophobic, wax-coated, and hydrophilic, nonwaxy regions. These uniquely optimized features that contribute to specific functions provide excellent sources of inspiration for human beings to create artificial surfaces by mimicking both the structues and functions of natural species.

Inspired from naturally fascinating features, people attempt to change a surface's wettability either by depositing the surface with a layer of chemical coating (e.g., fluoroalkylsilane) to reduce the surface free energy or by creating a hierarchically multiscale structure to enhance the surface roughness.[12] Although hydrophobicity can be enhanced by chemical modification that lowers the surface energy, a contact angle (CA) larger than 120° has never been achieved for water on flat surfaces.[13] In addition, some chemical layers have the drawback of a short-lived effect, which will deteriorate the hydrophobicity of treated surfaces over time. Very often, surface roughening together with chemical coating is employed to modify the surface wettability by producing ordered or disordered surface structures. Numerous techniques,[14,114] such as photolithography, nanocasting and extruding of polymers, block copolymers, vertically aligned carbon nanotubes, and electron-beam lithography, have been utilized to construct large-scale roughness on a large variety of surfaces. Despite their excellent performance, they suffer from some shortcomings, such as complexity (multiple steps), the need for an expensive mask, etc. A one-step fabrication technique, which can greatly reduce both the complexity and cost, is still desirable.

Recently, laser processing has emerged as a novel powerful approach for the modification of surfaces' wettabilities. This technique presents some unique advantages over traditional methods:[15] (i) It is a one-step direct maskless fabrication technique. A great number of hierarchical structures consisting of micro- and nanoscale features have been created, similar to those of natural species. Moreover, these structures can be

Received: May 5, 2013
Accepted: July 18, 2013
Published: July 18, 2013

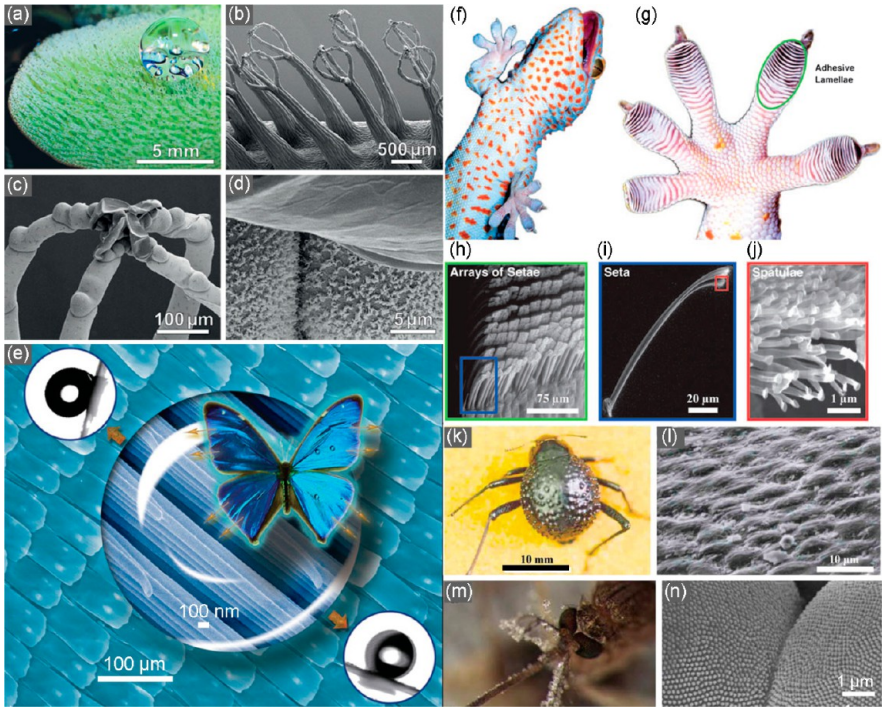

Figure 1. (a–d) Morphology of Salvinia molesta floating leaf.[7] (a) Upper side of the leaf surface densely covered with hairs. The spherical shape of the water drop on the leaf indicates the superhydrophobic character of the surface. (b–d) SEM images of the complex hair structures. (b) Four multicellular hairs grouped on top of an emergence and connected at the terminal end, leading to an eggbeater-shaped structure. (c) Collapsed terminal cell of each hair, forming a patch of four dead cells. (d) Whole leaf surface covered with nanoscale wax crystals (below) with the exception of the terminal cells (above). Reproduced with permission from ref 7. Copyright 2010 Wiley. (e) Directional adhesion of water on superhydrophobic Morpho aega (butterfly) wings.[9] The background image is the periodic overlapping microscales on the wings, while the image in the water droplet is fine lamella-stacking nanostripes on the scales. Reproduced with permission from ref 9. Copyright 2008 Wiley. (f) Macrostructure: ventral view of a tokay gecko climbing a vertical glass.[10] (g) Mesostructure: ventral view of the foot, with adhesive lamellae (scansors) visible as overlapping pads. Note the clean appearance of the adhesive surface. (h) Microstructure: proximal portion of a single lamella, with individual setae in a visible array. (i–j) Nanostructure: single seta with a branched structure at the upper right, terminating in hundreds of spatular tips. Reproduced with permission from ref 10. Copyright 2004 National Academy of Sciences, U.S.A. (k) Adult female, dorsal view. Peaks and troughs are evident on the water-capturing surface of the fused overwings (elytra) of the desert beetle Stenocara sp.[11] (l) SEM image of the textured surface of the depressed areas. Reproduced with permission from ref 11. Copyright 2001 Wiley. (m) Closeup of antifogging mosquito eyes after exposure to water aerosol.[8] The surfaces of the eyes remain dry and clear, while the surrounding hairs nucleate many drops. (n) SEM image of two neighboring ommatidia. Reproduced with permission from ref 8. Copyright 2007 Wiley.

modulated by changing processing parameters, including the scanning speed, pulse number, laser fluence, and laser polarization. (ii) It is a flexible technique without the need for a harsh machining environment. Experiments can be performed in vacuum and other gaseous atmospheres, such as air[24] and SF_6,[39] and liquid environments, such as water[26] and ethyl alcohol. It also does not require expensive clean-room facilities, thus greatly reducing the cost. (iii) It can greatly alter the wettability of certain materials even without the assistance of chemical coating to lower the surface free energy. (iv) It can be used for structuring a wide range of materials such as metals, glasses, and ceramics, especially applied to materials with hardness and high melting point or resistant to corrosion and brittleness. (v) The fabrication of true three-dimensional (3D) structures inside transparent materials is only possible by a nonlinear multiphoton absorption process of a high-intensity, femtosecond (fs) laser beam, thus allowing for their application in microfluidics and lab-on-chip devices. Meanwhile, in combination with a precise 3D computer number control (CNC) translation stage, fs laser micromachining provides a facile and efficient prototyping means.

The use of a laser system in modifying the wetting properties traces back to 1997 when various laser systems were available such as CO_2, a high-power diode laser, and Nd:YAG and UV excimer lasers. Lau et al. first reported that polyester fabric samples exhibited better hydrophobicity and dyeability at room temperature after excimer laser irradiation.[16] Since then, modification of the surface wetting properties by means of laser processing has become a new research branch and the influence of a variety of structures with respect to various materials on the surface wettability has been investigated.[17−21]

Although these laser systems can change the surface wetting properties, they face the challenge of producing more complex and prominent composite structures with better wettability. Traditional nanosecond (ns) laser systems have an apparent drawback of photothermal ablation, which brings about a large amount of molten material and produces a "corona" around the ablated hole.[22] Progress in technology has given rise to the invention of chirped pulse amplification and pulse compressor techniques, which give birth to a new fs laser system with ultrashort pulse (<1 ps) and high intensity. A comparison of the structures treated between the fs and ns/picosecond lasers demonstrates that fs laser micromachining can tremendously increase the precision of microstructuring due to many advantages, such as the very rapid creation of vapor and plasma phases, negligible heat conduction, and absence of a

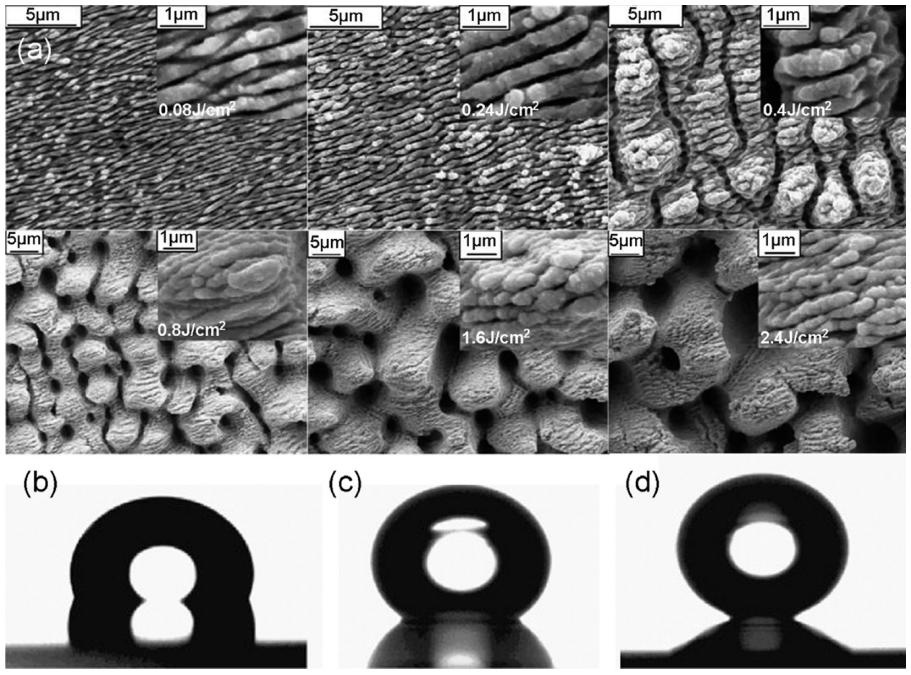

Figure 2. (a) SEM micrographs of AISI 316L type austenitic stainless steel based surfaces at various laser fluencies. (b–d) Photographs of water droplets on flat, LIPSS, and double-scale structures after silanization.[33] Reproduced with permission from ref 33. Copyright 2009 Elsevier.

liquid phase.[23] Therefore, fs laser micromachining opens up possibilities for a "delicate" material processing and microstructuring with enhanced precision. Despite being in its infancy, the outstanding ability of laser microfabrication has been paid more and more attention, and the relative findings per year grow very rapidly.

This paper provides an overview of employing lasers, especially a fs laser, to develop diverse wettabilities on a wide variety of materials. It first aims at describing related research performed so far, mainly focusing on how the wetting properties respond to different kinds of structures and where various wettabilities obtained by laser fabrication can be applied. It also serves to bridge a gap between different research fields, while proposing a promising application field for researchers who devote their energy to laser microfabrication, as well as making researchers in the face of difficulty in altering surfaces' wettabilities aware of a new technological route. The paper is organized as follows. In section 2, the main laser-structuring methods that have been applied to change the surface wetting properties are reviewed, including laser direct writing, laser interference lithography (IL), pulsed laser deposition (PLD), and laser textured templating. In section 3, unique advantages possessed by laser treatment to alter the surface wettability are introduced and the underlying mechanism responsible for the corresponding phenomenon is discussed. In section 4, numerous practically functional wetting surfaces based on laser fabrication are presented, including switchable wetting surfaces, biomimetic surfaces, and multiple biocompabible surfaces. Finally, the challenges and prospects within this topic are briefly discussed.

2. LASER FABRICATION METHODS USED FOR THE PREPARATION OF WETTING SURFACES

2.1. Laser Direct Writing. Laser direct writing is the most widely used approach for generating wetting surfaces because of its ease of setup and performance.[24] The resultant morphologies of laser structured surfaces depend on the exposure parameters (energy, pulse duration, repetition rate, wavelength, scanning speed, polarization, environment, etc.) and material properties (bandgap, thermal conductivity, etc.).[25−27] Generally, as-prepared structures can be classified into two categories in terms of utilized laser fluence.[28] For laser fluence near or just above the ablation threshold, a periodic nanoscale structure will turn up, known as laser-induced periodic surface structures (LIPSS), being first discovered by Birnbaum in 1965 after ruby-laser irradiation of various semiconductor surfaces.[29] LIPSS is a unique characteristic only possessed by laser irradiation. For higher laser fluence, a disruptive modification occurs, resulting in hierarchical micro- and nanoscale structures. Using different laser fluences, a large diversity of nano- or microstructures with different morphology, periodicity, and size can be developed.[30−32]

Recently, the wettability of a "ripple" surface composed of wavy surfaces with periodicity and amplitude equal to or smaller than the wavelength of the laser beam was investigated on steel (Figure 2a). The introduction of ripple structures on stainless steel elevated the CA of the flat surface from 113.0 ± 0.9° (Figure 2b) up to 150.3 ± 1.3° (Figure 2c) by enhancing the surface roughness.[33] The cone-shaped spike surface achieved at high fluence gave birth to CA = 166.3 ± 1.1° (Figure 2d), indicating that a hierarchical double-scale structure was superior to nanoscale LIPSS in enhancing the wettability performance.

Laser fluence is related to the number of pulses per irradiated spot. The thresholds of modification and ablation depend on the number of applied laser pulses. The threshold fluence $\Phi_{th}(N)$ for N pulses is related to the threshold fluence $\Phi_{th}(1)$ for $N = 1$ by a power law[34] $\Phi_{th}(N) = \Phi_{th}(1)\cdot N^{\xi-1}$. ξ is a material-dependent incubation coefficient. Because ξ is a value of less than 1, e.g., 0.84 of silicon,[35] the ablation threshold decreases with an increase in the number of pulses per irradiated spot because of the accumulation effect. A great

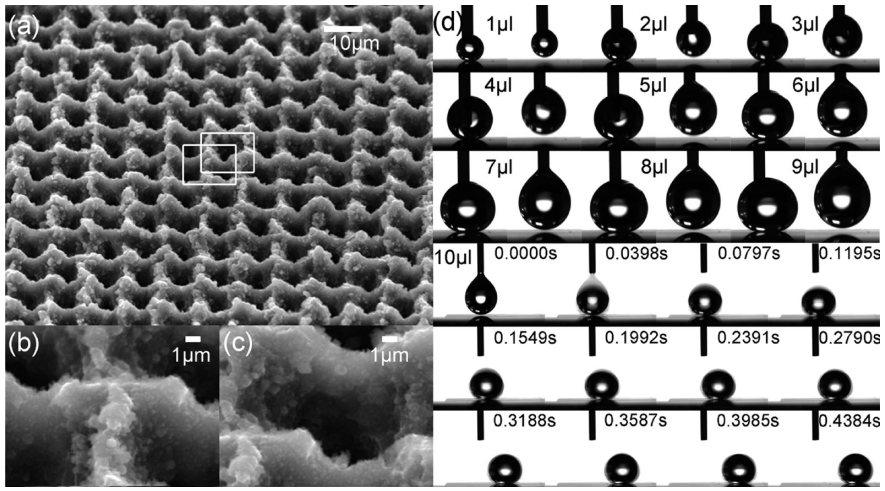

Figure 3. (a–c) SEM image of silicon irradiated by a fs laser.[24] (b and c) Corresponding magnification SEM images of specific locations. Reproduced with permission from ref 24. Copyright 2011 American Chemical Society. (d) Responses of 1–10 μL water droplets on the surface.[120] Reproduced with permission from ref 120. Copyright 2012 American Chemical Society.

change in the morphology of laser-achieved structures will take place with increasing N.[36] Jagdheesh et al. investigated the nanoscale ripples produced on stainless steel sheets at N = 12, 24, 36, and 48 and found that the center of the irradiated spot had undergone some melting and contours of a nearly flat surface formed as N increased.[37] Nanoscale protrusions formed between the regions of large ripples, whose quantity was found to increase with N. Therefore, increasing the number of pulses per irradiated spot would lead to an increase of the average roughness of the treated surface and therefore result in higher hydrophobicity. A similar trend also appeared on the poly(ethylene terephthalate) fiber,[38] where ripples emerged at a small amount of pulse exposure, then approached parallelism, evolved into an ellipsoidal segment, and finally turned out to be meander-like structures with more laser pulses applied.

Mazur et al. found that water and hexadecane droplets exhibited different wetting trends on the structured surfaces after fluorination. Structures changed dramatically from periodic structures to an array of cone-shaped spikes[39] when the fluence was increased from 2.2 to 9.0 kJ/m^2. The processes, such as refraction of laser light in highly excited silicon and interference of scattered and refracted light,[26,40] were considered to contribute to the formation of the structures. For water, the CA increased by 40° upon microstructuring with a minimum fluence of 2.6 kJ/m^2 and then remained close to 160°. Meanwhile, the sliding angle (SA) jumped abruptly from 30° at 2.6 kJ/m^2 to less than 3°. Both CA and SA at higher fluence were independent of the laser fluence, and both met the criteria for a superhydrophobic surface[14] in need of a CA larger than 150° and a SA of less than 10°. In contrast to water, the laser fluence had a significant effect on the wettability for hexadecane. The CA first increased as the laser fluence increased from 2.2 to 4.5 kJ/m^2 and then began to decrease. All of the CAs for hexadecane were less than those for water, whereas the SAs for hexadecane were around 30°, far larger than those of water. The disparity between water and hexadecane in the appearance of CA and SA was due to the difference of surface tension. Hexadecane has a lower surface tension, γ_{HD} = 26.7 mN/m, than water, γ_{H2O} = 72.0 mN/m, making a hexadecane droplet more apt to wet the structures and thus result in lower CAs and higher SAs than that of a water droplet.[41] A similar hydrophobicity-to-superhydrophobicity transition and subsequent water CA saturation trend was also observed by Stratakis's group,[42] originating from structure evolution at different fs laser fluences. The as-prepared superhydrophobic surfaces exhibited both self-cleaning and water-bouncing properties.[43]

Zhang et al. prepared an excellent superhydrophobic silicon surface with an extremely low adhesive force.[24] The fs laser structured domain was characterized by self-organized 10 μm periodic conical spikeforests with tens or hundreds of nanometer-sized protrusions (Figure 3a–c). A 9 μL water droplet was unable to land on the surface,[120] in which case the CA was considered to be close to 180°.[44] Only when the water dosage reached 10.0 μL did the droplet separate from a microsyringe under the gravitation effect, then fall on the slightly tilted sample, and instantaneously roll off (Figure 3d). Besides the metal and semiconductor, superhydrophobicity could also be realized on a K9 glass surface by introducing double-scale structures such as crater, ripples, and cones through fs laser irradiation.[45]

The wettability of an as-prepared surface often shows a dependence on the employed laser fluence.[46] However, some other interesting phenomena have also been discovered. De Marco et al. found that hydrophobic behaviors exhibited almost the same on poly(methyl methacrylate) (PMMA) surfaces at different laser fluences, which might be due to two reasons: lower roughness of the ablated area and removal of debris during the cleaning procedure.[47] On PMMA, increasing fluence would transfer a surface's wettability not only to hydrophobic (0.40–2.1 J/cm^2) but also to hydrophilic (2.1–52.7 J/cm^2).[48] The reason for this up–down transition of wettability[49] will be discussed in detail in the following section.

Besides the laser fluence and pulse number, the scan speed can also influence the topography and surface wettability by controlling spot overlap.[50] Circular grooves transformed into radial grooves with increasing scan speed, thus giving rise to a better wettability.[51]

Through analysis of the structures that are devoted to different wetting behaviors, it can be concluded that both micro- and nanostructures play a critical role in determining the final wettability.[11,14] The emergence of hydrophobicity and even superhydrophobicity after laser texturing can be explained by the Cassie–Baxter (suspension) model,[52] which assumes

that a liquid drop does not completely wet the structured surface but interacts with the composite surface made of a substrate material and air that is trapped in the crevices of the structured surface. For a rough surface containing only one type of asperities, the resultant CA can be calculated by the following equation: $\cos\theta_c = f(1 + \cos\theta) - 1$. f is the solid fraction, and then the air fraction is $1 - f$. The CA of air is 180°. Therefore, CA (θ_c) is the sole function of the solid fraction for a given surface with CA of θ. To obtain a superhydrophobic surface, the contribution of the solid part should be as small as possible.[53] An increase in the height of the structures with increasing laser fluence will lower the solid fraction of a droplet, thus resulting in high water repellency. What's more, the presence of nanostructures also plays an important role in the final wettability because single micro- or nanoscale features usually produce contact angle hysteresis (CAH) to some extent, even for a surface in Cassie's state.[54,55] The cooperation of microscale with nanoscale structures to form hierarchically multiscale structures will enable a droplet to anchor in the "lotus" state,[56] thus resulting in superhydrophobic surfaces with self-cleaning properties.

2.2. Laser IL. Laser IL is a facile, maskless, inexpensive, large-area nanolithography technique. The operation principle of this technique is simple: when two or multiple pulses overlap in time and space, an interference pattern turns up. By changing interfering beams' number and direction, amplitude, phase, and polarization, surfaces can be precisely and spatially modified into a large variety of periodic one-dimensional (1D), two-dimensional (2D), and 3D patterns with different sizes and shapes for various applications.[57,58] Brueck et al. have reviewed IL technology and diverse applications for nanostructures and functional materials based on IL, involving the directed self-assembly of colloidal nanoparticles, nanophotonics, semiconductor material growth, and nanofluidic devices.[59] Thomas et al. summarized the fabrication of 3D structures via IL (e.g., the formation of interference patterns, their dependence on beam parameters, and several requirements for the photoresist, PR), along with a brief review of the applications of 3D structures in photonic and phononic crystals, as microframes, and for the synthesis of highly nonspherical polymer particles.[60]

On the basis of fs laser IL, a submicrometer-scale periodically grooved structure was fabricated on azobenzene-containing polymer films, on which a droplet exhibited anisotropic wetting properties,[61] displaying different CAs measured from orthogonal directions. The surface wettability showed a disparate dependence on the depth and period of the groove that could be adjusted by altering the fluence and incident beam angle, respectively. The CA (~83°) measured from the perpendicular direction was almost independent of the groove depth, nearly equal to those on flat surfaces (82°) all of the time, while the CA measured from the parallel direction was dependent on the groove depth, based on which the degree of wetting anisotropy could be modulated from 2.1° to 13.7°. Sun et al. utilized improved four-beam laser IL to develop a series of novel Micropearl arrays with the ability to control both the CAs in orthogonal directions by adjusting the thickness of resin and the intensity ratio of four laser beams.[62]

Strongly anisotropic wetting phenomena were observed on a 1D grooved surface of both positive and negative PRs.[63] The plasma treatments with different gas compositions (e.g., CHF_3, CF_4, O_2) and polymer deposition were employed to tailor anisotropic wetting properties from strongly anisotropic and hydrophobic to hydrophobic with very high CAs and superhydrophilic with a smaller degree of anisotropy. The degree of anisotropy $\Delta\theta$ of negative/positive grooved PRs (800 nm pitch density, ~500 nm depth, and ~300 nm narrow channels) changed from 74°/81° to 19°/32° after CHF_3 or CF_4 plasma treatment (Figure 4a–d). The change in the surface wettability resulted from an increase of the fluorine (F) content after CHF_3 or CF_4 treatment. In addition, spin-coating deposition of a silica nanoparticle suspension atop the PR structures could reduce both anisotropy and hydrophobicity.[64] The anisotropic and hydrophobic surfaces (θ_x = 130°; θ_y = 51°; $\Delta\theta$ = 79°) converted into a less anisotropic hydrophilic surface (θ_x = 38°; θ_y = 8°; $\Delta\theta$ = 30°) for a 1500-nm-period sample (Figure 4e–h).

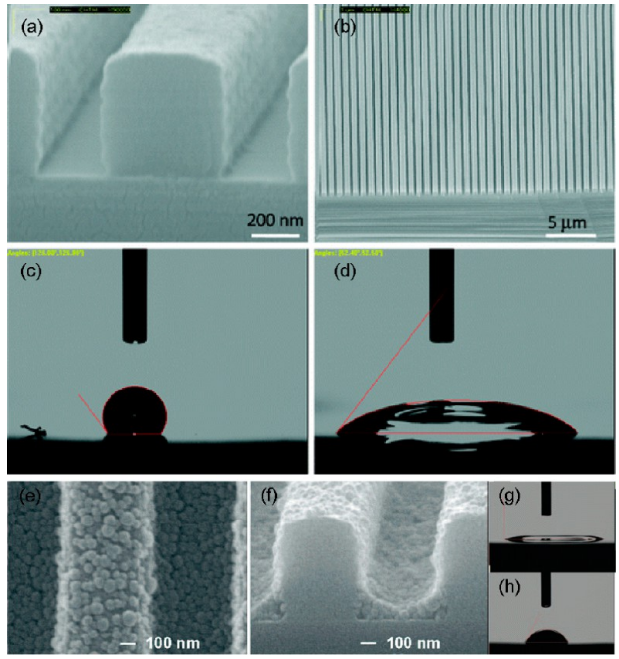

Figure 4. SEM images (a and b) and CAs (c and d) on a negative PR pattern with 800 nm pitch density, ~500 nm depth, and ~300 nm narrow channels.[63] Reproduced with permission from ref 63. Copyright 2010 American Chemical Society. SEM images (e and f) and CAs (g and h) on a 1500-nm-period sample modified by spin coating with a 5 wt % silica nanoparticle suspension.[64] Reproduced with permission from ref 64. Copyright 2008 American Chemical Society.

Cooperation of IL with other techniques can enrich the diversity of as-prepared structures.[65] Sun et al. produced three kinds of superoleophobic surfaces (20 μm pitch micropillar arrays, 2.5 μm pitch micropillar arrays, and gecko footlike hierarchical microstructures) by combing laser interference, spin coating, photolithography, PDMS transfer, and O_2 plasma treatment techniques.[66] The hierarchical surface with high surface roughness showed extreme underwater superoleophobicity with distinct adhesive behaviors. Sun et al. also successfully utilized multibeam interference followed by an electroless-plating technique to endow a surface with superhydrophobicity.[67] The former technique was employed to pattern regularly hydrophobic microneedle or microrod arrays; the latter one was used to form additional nanoscaled features (20–50 nm silver particles) on microscale surfaces to generate hierarchical structures, resulting in superhydrophobicity with CAs as high as 163 ± 2°.

Table 1. CAs of Different Materials before and after Laser Ablation

material	original CA	treated CA	CA enlargement	ref
silicon	66°	131°	65°	88
silicon	64.2°	97.5°	33.5°	79
silicon/silicone elastomer	64°/110°	130°/159°	46°/49°	134
Ti6AlV/AISI 316L stainless steel	75°/79.5°	124.6°/116.5°	49.6°/37°	89
316 stainless steel	68.5°	130°	61.5°	90
Ti64V, steel AISI 304L/630/4140/M2/P20	60−85°	110−153°	50−68°	96
ZrO_2	72°	151°	79°	97
PMMA	74.1°	107°	32.9°	47
PS	82°	150°	68°	93

2.3. PLD. The PLD technique is capable of growing high-quality thin films, such as Co−B[68] and Zn0.9Co0.1O.[69] A typical experimental setup of PLD is illustrated in ref 70. A target in a vacuum chamber is irradiated by a laser. Some of the target material will be moved, which will then grow on the films with thicknesses in the sub-nanometer to micrometer range. The films can be produced not only in a high vacuum but also in a reactive background gas, such as oxygen, nitrogen, and argon. PLD is a versatile and powerful tool for producing nanoparticles with desired size and composition only by varying the experimental deposition conditions.

Daoud et al.[71] utilized PLD to deposit poly(tetrafluoroethylene) (PTFE) thin films on cellulosic cotton substrates at room temperature to enhance the wettability from CA = 0° to 151°. Wong et al.[72] deposited PTFE on glass substrates by PLD to fabricate an excellect superhydrophobic surface with a CA of 170° and a SA of less than 2°. Koshizaki et al.[73] combined PLD with an annealing process to fabricate ordered Co_3O_4 hierarchical nanorod arrays. Before fluorosilane coating, the as-prepared Co_3O_4 nanorod arrays exhibited superior superhydrophilicity without UV irradiation because of the improved roughness and the presence of abundant OH− groups. After chemical modification to reduce the surface free energy, the surfaces turned out to be hydrophobic or superhydrophobic with controlled water CAs. They also prepared a hierarchical TiO_2 ordered hemispherical particle array with hexagonal non-close-packed tops and hematite hierarchical columnar arrays by replicating a polystyrene (PS) colloidal monolayer through the PLD process.[74−76] All of these hierarchical particle arrays exhibited excellent superhydrophilicity (CA ≈ 0°) without UV irradiation.

2.4. Laser Textured Templating. Polymers, including poly(dimethylsiloxane) (PDMS), PMMA, PS, and cycloolefin polymer, possess a number of advantageous properties such as flexibility, durability, transparency, chemical inertness, and good biochemical compatibility that make them more attractive in the design and fabrication of polymer-based microfluidic devices. Casting polymers from a mold and subsequent bonding to a flat PDMS counterpart provide a very rapid fabrication method for enclosed microfluidic devices.[77]

The wettability of polymer structures is an important aspect for polymer-based microfluidic devices to be used at different regions.[78] Wu et al. generated biomimetic hierarchical structures to mimic the lotus leaf's surface by combining templating, laser direct ablation, and nanodecoration.[79] The laser textured silicon structures elevated the wettability from hydrophilic (flat silicon, CA = 64.2°) to hydrophobic (97.5°). After imprinting a laser-induced structure onto a sol−gel film, the CA of the imprinted sol−gel film surface increased by nearly 30° up to 138° because of the introduction of the two-tiered roughness of patterned silicon. The hydrophobicity of imprinted sol−gel surfaces could be further enhanced into superhydrophobicity with CA of 160.3° and CA hysteresis of 0.9° by the coating of nanoparticles.[80]

A great diversity of morphologies achieved by altering linear/circular polarization, the laser fluence, and the scanning speed offer a powerful template platform. Wu et al.[81] investigated the wetting performance of templates of periodic-like nanostructures or nanostructure-covered conical microstructures of STAVAX steel irradiated by fs laser pulses. After thermal injection molding, an improvement of about 6−9° in the CA for low laser fluence and about 36−37° for high laser fluence in comparison with CA = 97° of flat polypropylene were observed. Glass plate,[82] PDMS, PMMA, and PS[83] can also act as a template master. For example, Jeoung et al.[84] investigated positive and negative replication of a fs laser structured PDMS surface, which consisted of an irregular 3D papilla structure on the order of micrometers with 3−300 nm nanostructure decoration. The modified surface showed superhydrophobicity with a CA higher than 170° and a SA of less than 3°. The positive replica maintained superhydrophobicity, while the negative replica exhibited large CAH with a SA of 90° and a lower CA of 136°.

3. UNIQUENESS OF LASER TREATMENT

3.1. Directly Induced Hydrophobicity or Superhydrophobicity. The material surface energy plays a prominent role in determining adhesive interactions between a droplet and the substrate it anchors. Reducing the surface energy chemically, topographically, or both will lower the adhesive force of a surface and therefore increase the surface's hydrophilicity to hydrophobicity or even to superhydrphobicity. Depositing a hydrophobic coating on the top of a textured surface is often employed.[85,86]

fs laser ablation provides an alternative method to significantly change the surface wettability by only producing multiscale structures without the need for additional chemical coating.[87] Table 1 shows the CAs before and after laser ablation with respect to different materials. Zorba et al.[88] found that the CA increased from 70° to around 131° and saturated at this value, with the fluence increasing from 0.17 to 1.0 J/cm^2. Wang et al.[79] observed that, with an increase in the pulse number, the CAs of the silicon surface increased from 64.2° (smooth) to a maximum of 97.5° at four pulse irradiations by UV laser irradiation and then decreased to about 76° with a further increase in the pulse number. Benayoun et al.[89] reported a similar wetting transition trend on AISI 316L stainless steel. After fs laser irradiation, the CA of structured steel increased from 79.5° (smooth surface) to a maximal value of 116.5° at N = 84 pulses and decreased to 86° at N = 128. As for Ti6AlV, an

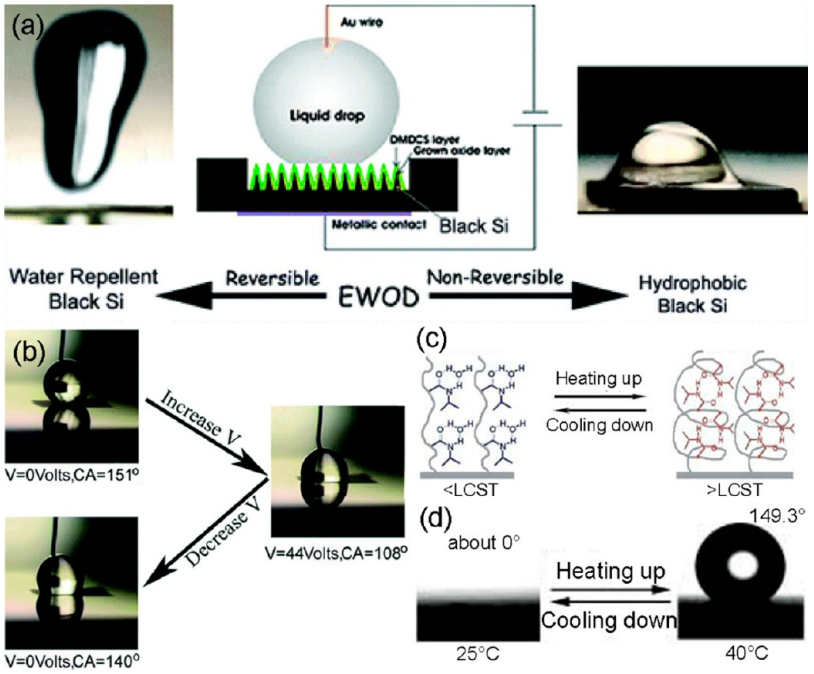

Figure 5. (a) Schematic electrowetting-on-dielectric (EWOD) system for structured silicon substrates. (b) Reversibility of an EWOD system based on a superhydrophobic black silicon surface.[106] Reproduced with permission from ref 106. Copyright 2010 American Chemical Society. (c) Diagram of the reversible formation of intermolecular hydrogen bonding between PNIPAAm chains and water molecules (left) and intramolecular hydrogen bonding between C═O and N−H groups in PNIPAAm chains (right) below and above the LCST, which is considered to be the molecular mechanism of the thermally responsive wettability of a PNIPAAm thin film.[110] (d) Water drop profile for thermally responsive switching between superhydrophilicity and superhydrophobicity of a PNIPAAm-modified rough surface with a groove spacing of about 6 mm, at 25 and 40 °C. The water CAs are about 0° and 149.3 ± 2.5°, respectively. Reproduced with permission from ref 110. Copyright 2003 Wiley.

increase in the pulse number would lead to a gradual increase of CA from 75° (smooth surface) to 124.6° at N = 128. The CA of 316 stainless steel could also be enlarged from 68.5° to 130.0° by introducing periodic grooves with different ratios of clearance between two grooves and the width of the grooves.[90]

The wettability is sensitive to surface chemistry changes, especially the oxygen atomic percentage. Lam et al.[48] found that fluences from 0.40 to 2.1 J/cm^2 produced a hydrophobic surface and those from 2.1 to 52.7 J/cm^2 produced a hydrophilic surface. X-ray photoelectron spectoscopy (XPS) spectra demonstrated that high fluence produced the highest concentration of polar group O 1s O═C and the lowest concentration of nonpolar group C 1s C−C, thus resulting in high hydrophilicity. In contrast, the surface subjected to low fluence had the highest concentration of nonpolar group C 1s C−C and a low total concentration of polar groups compared to the raw PMMA surface, resulting in increased hydrophobicity. Farson et al.[91] found that scaffold surfaces ablated in ambient air or flowing oxygen increased the atomic oxygen percentage and oxygen-containing group fractions, therefore leading to smaller CAs compared to those on untreated surfaces. In short, the fraction of oxygen-containing groups is negatively related with the sessile-drop CA because of their strong affinity for hydroxylation, whereas the percentage of non-oxygen-containing groups is positively correlated with the wetting angle.[92] The atomic oxygen percentage, especially the ratio of O/C, determines the resultant wettability of the laser-treated surface. A decrease in the atomic oxygen percentage is favorable for increased surface hydrophobicity.[93−95] Hatzikiriakos et al.[96] reported that the transition of wettability from hydrophilic (60−85°) to hydrophobic and even superhydrophobic (110−153°) did not happen just after laser irradiation. It was a slow process needing several days. XPS analysis revealed that the change in the wettability correlated with the presence of carbon and its compounds on the structured surface. The introduction of carbon not only came from a fast decomposition reaction at the time when the laser pulses hit the surface but also originated from a slow and nonpolar CO_2 decomposition reaction on the latter irradiated surface.

However, not all direct wettability enhancement by means of laser irradiation is attributable to the deficiency of the oxygen percentage; some of them may come from the roughness of structures. For example, the CA of ZrO_2 increased from 72° (smooth substrate) to approximately 151° with increasing laser fluence.[97] XPS revealed that laser irradiation did not lead to the deficiency of lattice oxygen, so the laser-induced structure should play a dominant role in the hydrophobic property. In addition, after laser ablation, PMMA wetting behavior switched from moderately hydrophilic (CA = 74.1 ± 1.3°) to hydrophobic (CA = 107°), independent of the above-threshold laser fluence.[47] Although the peaks of C−O and C═O emerged for the sample ablated at maximum fluence, the atomic C/O ratio did not vary with the irradiation fluence. The change in wettability could only be imputed to the morphology of the substrate. Similarly, Mazumder et al.[98] attributed hydrophilic surfaces with CAs of less than 30° achieved by low-fluence irradiation to the higher presence of oxide of microcone structures compared to the polished surface, whereas for the high fluence, the wettability showed a wide wetting scale ranging from superhydrophilic (CA ∼ 0°) to hydrophobic (113°) dependent on the scanning speed. The emergence of hydrophobicity was due to the high aspect ratio

of microcones that prevented full penetration of the liquid into valleys between them.

3.2. Debris' Effect. In order to obtain artificial superhydrophobic surfaces, a great variety of pillar-type surfaces in micro- or nanoscales or both have been prepared. Through evaluation of the effect of the structure scale on wettability, it is found that the average value of the CAs measured from hierarchical structures (microstructures with nanoprotrusions) is higher than that measured from microstructures without nanoprotrusions.[99−101] The presence of secondary nanoprotrusions can greatly decrease the contact area between a water droplet and the surface it sits on, causing CAs to increase and CAHs to decrease effectively. The introduction of nanostructure inevitably needs additional processing after fabrication of microscale structures, which will increase both the complexity and cost of fabrication.

During the laser ablation process, large amounts of nanoscale debris are generated,[102] which could deposit on microscale structures to increase the surface roughness and increase the hydrophobicity. Berendsen et al.[103] reported that, with the assistance of redeposition of nanoscale debris on microscale square protrusions during laser ablation, CAH decreased from 27.8° of microstructures to 0.7° of the surface containing both microstructures and nanoroughness.

Normally, the strips' surfaces will elongate a droplet because of differences of the energy barriers exerted by anistorpic structures in orthogonal directions.[61] However, Jiang et al.[44] found that anisotropic surfaces showed perfect isotropic superhydrophobicity without apparent CAH, water adhesion, and drag resistance. By analysis of the surface's morphology, rugged nanoprotrusions between microstrips originating from debris deposition were found to elevate 2D roughness into ideal 3D roughness. The introduction of nanoparticles diverted "area" contact into "point" contact, thus greatly reducing the liquid−solid contact area and making the triple-phase contact line become extremely discrete.

4. APPLICATIONS

4.1. Smart Surfaces with Switchable Wettability. Smart surfaces with responsive switchable wettability[104] have drawn extensive interest because of their promising properties and wide range of potentially industrial applications, such as self-cleaning surfaces, microfluidic devices, controllable drug delivery, smart membranes, and so on. A large number of stimuli, including light illumination, temperature, solvents, electrical potential, pH, and others, can change the chemical conformation or polarity of a surface, thus resulting in a change of the surface wetting behavior.[105]

Recently, researchers have attempted to develop smart responsive switchable surfaces driven by various kinds of external stimuli via laser fabrication. For example, Stratakis et al.[106] reported a kind of electricity-responsive switchable surface. By application of moderate external electric fields, a glycerol droplet on fs laser-induced spike surfaces could be readily switched between superhydrophobicity and hydrophilicity. Parts a and b of Figure 5 show the snapshots of glycerol droplets on the surface prepared at 1.69 J/cm^2 at different voltages. The CA at 0 V equaled 151°, then dropped down to 108° at 44 V, and returned to 140° when the voltage was reduced to 0 V. The reversibility depended on the patterned structures and water-repellent characteristics of the surfaces. It was apparent that the pronounced double-scale roughness obtained at high fluence had small values of CAH.

As one class of photosensitive materials, many metal oxides, such as TiO_2, ZnO, SnO_2, WO_3, V_2O_5, and Ga_2O_3, can be switched between two different wettabilities when they are alternatively exposed to ultraviolet (UV) light and stored in the dark.[107] Covering the fs laser-induced silicon spikes with ZnO nanoprotrusions enabled a liquid droplet to rapidly and reversibly switch between hydrophobicity and superhydrophilicity.[108] The samples exhibited a significant photoinduced transition to superhydrophilicity, reaching nearly 0° CA in a short time. Both dark storage and thermal heating could reconvert superhydrophilic surfaces to their original hydrhophobic states within 24 h. It should be noted that thermal heating at 200 °C for 1 h could speed the reversibility process of all surfaces to their original hydrophobic state. Numerous switching cycles of each sample would not deteriorate the irradiation efficiency or reversibility behavior. The reason for the photoinduced transition is due to the electron−hole pairs in the ZnO lattice generated by UV irradiation. Some of the holes react with lattice oxygen to form surface oxygen vacancies, while electrons react with metal ions (Zn^{2+}) present in the lattice, forming Zn^+ defective sites. Meanwhile, water and oxygen may compete to dissociatively adsorb on these vacancies. The Zn^+ defective sites are kinetically more favorable for hydroxyl adsorption than oxygen adsorption. As a result, the surface hydrophilicity is improved, and the CA is significantly reduced.

Some efforts have been devoted to the development of surfaces functionalized with photochromic molecules because of their reversible wettability change upon light irradiation.[109] When a SP-doped PMMA sample was irradiated by UV pulses, SP molecules converted to their merocyanine (MC) isomers and the surface became colored. Because MC stereoisomers exhibited an enhanced dipolar moment compared to that of SP isomers, the sample became more hydrophilic and thus the CAs decreased. Subsequent irradiation of the sample with green laser pulses converted the molecules back to its initial SP form and led to the return or better of the original CAs. The maximum differences between the average CAs measured before and after wetting transition on the flat/laser-induced roughness surfaces were 7 ± 1° and 19 ± 3°, respectively.

Jiang et al.[110] reported that laser-enhanced roughness (square silicon microconvexes with different spacings between the grooves) on the thermally responsive material of a poly(*N*-isopropylacrylamide) (PNIPAAm) surface could significantly enhance the degree of thermally responsive wettability to realize reversible switching between superhydrophilicity and superhydrophobicity (Figure 5c,d). As for the flat PNIPAAm-modified surface, the CA could only change from 63.5 ± 2.6° to 93.2 ± 2° with increasing temperature from 25 to 40 °C. As for the samples with spacings (D) of 31, 18, 8, and 6 μm, the water CAs were 33.5 ± 1.4°, 10 ± 0.6°, and ≈0° (8 and 6 μm) at 25 °C, respectively. At 40 °C, the water CAs of these surfaces were 112.9 ± 2.68° (D = 31 μm), 128.9 ± 1.4° (18 μm), 137.9 ± 2° (8 μm), and 149.3 ± 2.5° (6 μm), respectively. As discussed above, the decrease in the atomic oxygen percentage is favorable for increasing the surface hydrophobicity. Therefore, the processing environment can be another alternative approach to achieving switchable wettability. Annealing of the laser-irradiated sample at an O_2 atmosphere can introduce oxygen-related defects with high surface free energy, thus leading to a dramatic decrease of the CA of the surface. Subsequent exposure of the sample at ambient atmosphere can cause the CA to gradually reconvert to its original value.[97]

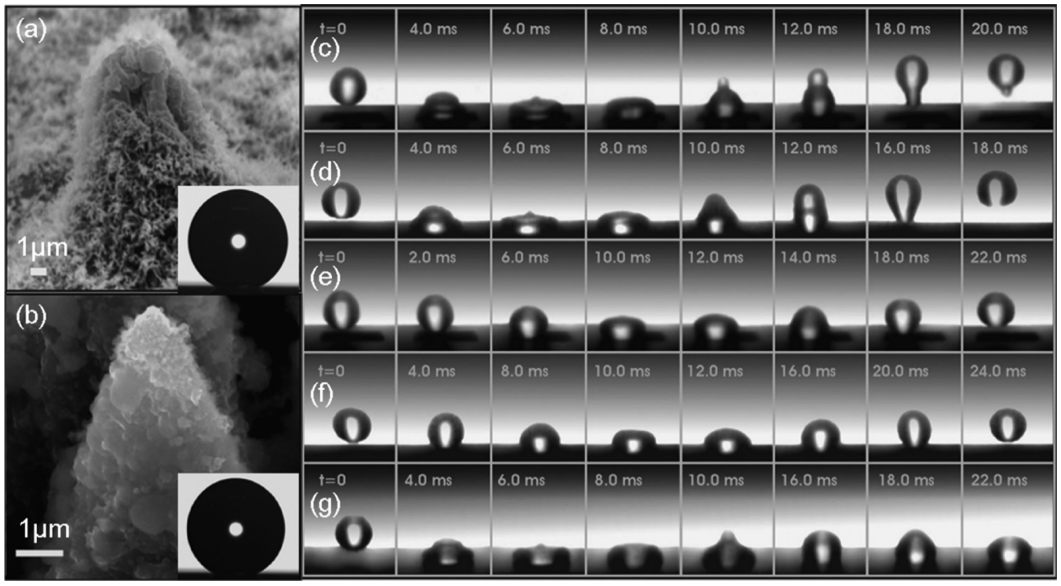

Figure 6. Comparison of the structure and droplet rebounce between the lotus leaf and fs laser structured silicon surface.[115] (a) High-magnification SEM image of a single papillose depicting branchlike protrusions with sizes of about 150 nm. The inset image shows water CA = 153 ± 1° of a droplet of 0.78 mm radius on the lotus leaf surface. (b) High-magnification SEM image of a single protrusion depicting nanostructures of sizes up to a few hundred nanometers on the slopes of the protrusions. The surface was structured in the presence of 500 Torr SF_6 at a laser fluence of 2.47 J/cm^2 with an average of 500 pulses. The inset image shows water CA = 154 ± 1° of a droplet of 0.78 mm radius on the lotus leaf surface. (c–g) Selected snapshots of the impact and rebound of millimetric water droplets: (c) on an artificial silane-coated structured silicon surface impacting with a velocity that corresponds to a *We* of 3.5; (d) on a lotus leaf surface impacting with *We* = 3.5; (e) on an artificial silane-coated structured silicon surface impacting with *We* = 0.7; (f) on a lotus leaf surface impacting with *We* = 0.7; (g) on an unstructured silane-coated silicon surface impacting with *We* = 3.5. Reproduced with permission from ref 115. Copyright 2008 Wiley.

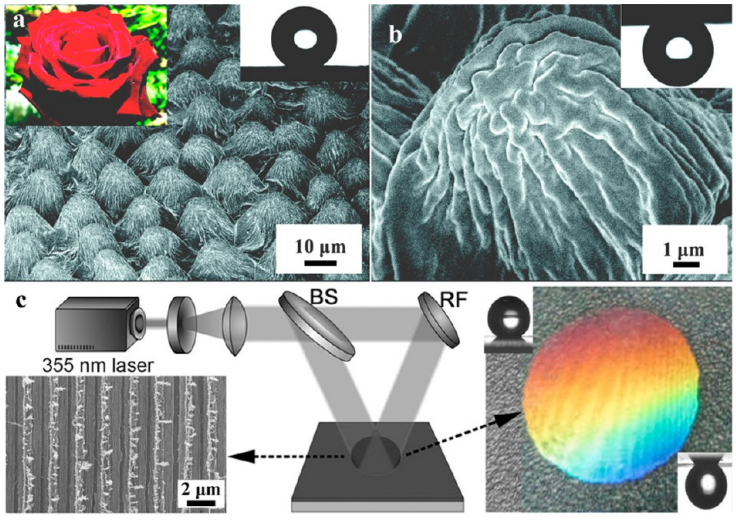

Figure 7. (a and b) SEM images of the surface of a red rose petal, showing a periodic array of micropapillae and nanofolds on each papillae top. The inset image of part a is the shape of a water droplet on the petal's surface with a CA of 152.4°, and that of part b is the shape of water on the petal's surface when it is turned upside down. Reproduced with permission from ref 116. Copyright 2008 American Chemical Society. (c) Fabrication scheme of biomimetic graphene surfaces by two-beam laser interference.[117] The image on the left is a SEM image of the grating structure of the graphene surface fabricated at 0.3 W, and the one on the right is a photograph of the graphene surface with iridescence. Inset images are the morphologies of a water droplet on biomimetic graphene surface with tilt angles of 0° and 180°. Reproduced with permission from ref 117. Copyright 2008 Wiley.

In addition to smart surfaces with stimili-responsive wettabilities, some surfaces possess self-controllable wettabilities without the need for external stimuli. Zhang et al.[111] found that directional triangular structures fabricated by a fs laser had the ability to realize mutual wetting transitions between anisotropic and isotropic. The reason for this phenomenon may be that a water droplet prefers to spread in the direction with less free energy.[112] When a droplet is in an anisotropic state, it will jump back along the direction with less free energy and subsequently returns to an isotropic state. Additionally, the authors have also found that an anisotropic water droplet on parallel strips patterned by a fs laser could also change to isotropic because of the droplet's collapse into adjacent strips

by conquering the energy barrier exerted by strips with increasing droplet volume.[24]

Jiang et al. reported a novel curvature-driven in situ switching for reversible tuning of the surface superhydrophobicity from the pinned to the roll-down state.[113] A PDMS surface with a regular array of pillars was prepared by IL and PDMS imprint lithography. The PDMS pillar-array film's CA was 150°, but it showed a very high adhesion force (56 mN) to hold a droplet even when the sample was turned upside down. When the surface curvature was increased from 0 to 0.62 mm^{-1}, not only did the CA slightly increase (up to 160°) but the adhesion force (12.5 mN) and SA decreased significantly (SA < 5°). Transformation between roll-down and pinned superhydrophobic states could be reversibly switched many times by changing the surface curvature. On the basis of the "switch" behavior, a "mechanical hand" could be realized to transport a water droplet without any loss.

4.2. Biomimetic Surfaces. In nature, many plants exhibit remarkable water-repellent properties. One of the most well-known surfaces is the lotus leaf and its self-cleaning effect,[6] which is attributed to its dual-scale hierarchical structure of papillose epidermal cells and an additional layer of epicuticular waxes. The papilla protrusions can greatly reduce the contact area between the lotus leaf and a liquid drop (or a particle), enabling a droplet to only reside on the tips of epicuticular wax crystals on top of papillose epidermal cells. Through a slight tilting, a droplet on the lotus leaf will roll off to carry contaminated particles away.

Mimicking superhydrophobic biosurfaces is always carried out to fabricate similar hierarchical structures on hydrophobic materials or on the hydrophilic surface followed by the coating of a chemical layer to reduce its surface energy.[114] Stratakis et al.[115] prepared artificial surfaces by fs laser irradiation of a silicon surface under a reactive gas atmosphere, which could quantitatively mimic both the structure and the water-repellent characteristics of a natural leaf of Nelumbo nucifera (lotus leaf). These surfaces were composed of microscale conical features with nanoscale protrusion decoration. The conical or pyramidal asperities' average size was around 10 μm (Figure 6b), almost equal to the 5−10 μm size of randomly distributed papillae on the lotus leaf (Figure 6a). The water CA and CAH of the artificial surface were 154 ± 1° and 5 ± 2°, respectively, both very close to 153 ± 1° and 4 ± 2° of the lotus leaf. Great similarities in the water repellency were also observed between the artificial surfaces and the lotus leaf in terms of droplet bouncing behaviors with a different dimensionless Weber (We) number (Figure 6c−g).

Besides the lotus leaf, the red rose petal is another branch of the superhydrophobic surface, on which a droplet has both large CA (>150°) and large SA values.[116] A droplet will stick to the surface when the petal is turned upside down (Figure 7a). The reason for this unique adhesive superhydrophobicity is its special microstructures and corresponding size compared to those on lotus leaves. The rose petal is composed of periodic micropapilla arrays of 16 μm diameter and 7 μm height. In addition, nanoscale cuticular folds of about 730 nm width decorate the top of the micropapillae (Figure 7b). The combination of micro- and nanostructures endow rose petals with high CAs for enough roughness. However, compared to the lotus leaf, the size of the hierarchical micronanostructure on the rose petal is much larger, causing a water droplet to enter into larger grooves of the rose petal and thus giving rise to a high adhesive force. Zhang et al.[117,118] fabricated a rose-petal-like superhydrophobic graphene surface with high adhesion by fs laser IL. The surface was composed of periodically hierarchical micronanostructures, as shown in Figure 7c. The surface's water CA (~157°) and wetting behavior were both similar to those of the rose petal. Interestingly, as is directly observed by the naked eye, the as-prepared graphene surfaces took on a wonderful iridescent appearance throughout the exposed area, matching the shape of the round laser spot (right image in Figure 1c). By the introduction of periodic triangular patterns between fs laser irradiated silicon grooves, a high adhesive force as well as anisotropic wetting could also be achieved simultaneously.[119]

Inspired by both the lotus leaf and rose petal, intense interest has been focused on smart superhydrophobic surfaces that exhibit tunable adhesive forces between the lotus leaf and rose petal. Zhang et al.[120] successfully fabricated a series of tunable adhesive superhydrophobic silicon surfaces consisting of periodic hydrophobic patterns (triangle, circle, and rhombus) and superhydrophobic structures (dual-scale spikes induced by a fs laser) via fs laser micromachining and fluorination coating. Through an increase in the area ratio of the superhydrophobic domain to hydrophobic domain, both the static and dynamic wetting properties could be modulated. The minimum water droplet volume that enabled a droplet to land on the surface could be tailored from 1 to 9 μL. The SA can be flexibly adjusted from >90° (rose-petal-like) to 5° (lotus-leaf-like). In addition, droplet rebound behaviors could also be modulated from partial rebound to multiple rebounds. These results demonstrated that hydrophobic domains actually contributed to the water adhesion force while superhydrophobic domains contributed to the water-repellent force. The adjustment of the ratio of the hydrophobic domain to superhydrophobic domain could tune the adhesive force of the surfaces.

Rice leaf[55] is famous for its anisotropic wettability because of its directional structures. The papillae are arranged in 1D order parallel to the leaf edge (direction of arrow) but randomly distributed in the other direction (perpendicular to the arrow), as shown in Figure 8c. On the rice leaf, a water droplet is nearly spherical along both directions and only shows a little anisotropy with θ_2 and θ_1 of 146 ± 2° and 153 ± 3° (Figure

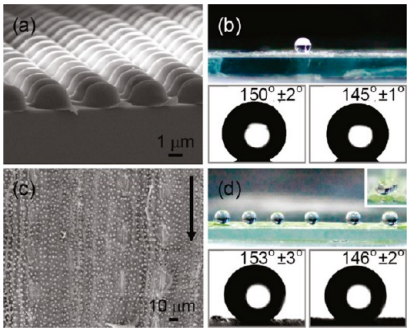

Figure 8. Comparison of biomimetic anisotropic surfaces and a natural rice leaf.[62] (a) Cross-sectional SEM image of Micropearl arrays with height variations of 1.75 μm/2 μm. (b) Digital photograph of a water droplet on modified Micropearl arrays (upper figure); CAs enhanced by (fluoroalkyl)silane modification (lower figure). (c) SEM image of a natural rice leaf. (d) Digital photographs of a water droplet on the rice leaf along both directions and the CA measurement showing that the designed anisotropy (145 ± 1° and 150 ± 2°) is close to those of the natural one (146 ± 2° and 153 ± 3°). Reproduced with permission from ref 62. Copyright 2010 American Chemical Society.

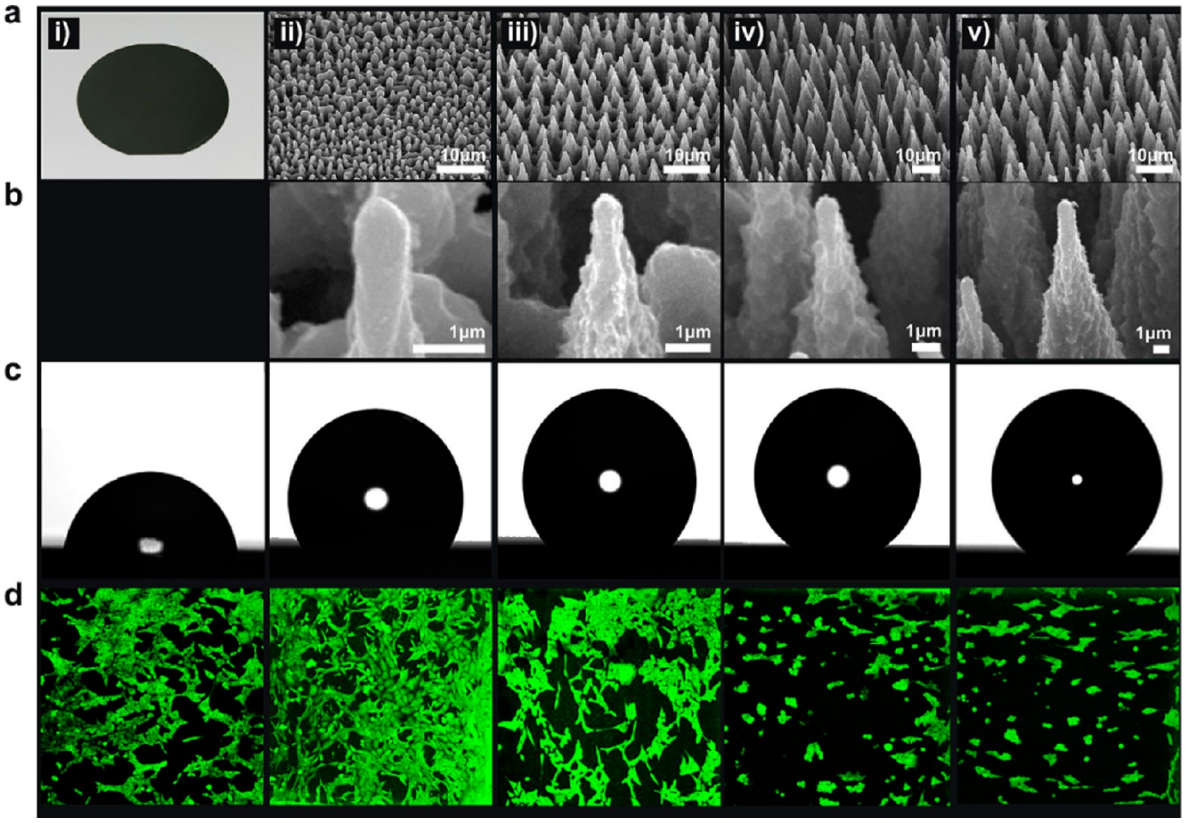

Figure 9. (a) Picture of a polished silicon wafer (i) and side views of SEM images of the as-prepared silicon spike structured surfaces at four different laser fluences: (ii) 0.34 J/cm^2 (A1); (iii) 0.56 J/cm^2 (A2); (iv) 0.90 J/cm^2 (A3); (v) 1.69 J/cm^2 (A4). (b) High-magnification SEM images of the corresponding silicon cones obtained. (c) Photographs of water droplets on the patterned silicon surfaces. (d) Confocal laser microscopy pictures of fibroblast cells cultured for 3 days on the respective surfaces.[133] Reproduced with permission from ref 133. Copyright 2010 Elsevier.

8d). A large value in the CA is beneficial for the rice leaf to control the motion of water droplets. The SAs for a water droplet to roll along the direction of the arrow are 3−5° and 9−15° perpendicular to the arrow, thus allowing droplets to roll off along a certain direction. Many researchers are devoted to the fabrication of rice-leaf-inspired surfaces with anisotropic wettability.[121,122] Through IL and low-surface-energy modification, an artificial anisotropic surface consisting of Micropearl arrays (Figure 8a) was developed to mimic the rice leaf with CAs in orthogothal directions of 145 ± 1° and 150 ± 2° (Figure 8b), both very close to those of the rice leaf.[62]

4.3. Cell Manipulation. Various materials have been engineered to modulate cell−biomaterial interactions because cell adhesion, growth, division, and migration are highly dependent on their immediate culture substrate.[123−125] Like the case in the wetting surface, both the surface roughness and surface chemistry play critical roles in determining cellular behaviors on a biomaterial surface. Apart from these two factors, the wettability is another important factor influencing cellular behaviors on the structured surfaces.[126−128] Several efforts have been undertaken to manipulate the cellular behavior by altering the surface topography, chemistry, and wetting properties to create an "intelligent" biomaterial. Laser fabrication has been widely used to fabricate diverse surface topographies on a large variety of surfaces to realize selective cell control via proliferation.[129−131] However, integration of roughness with wettability to tune cellular behaviors by means of laser fabrication is still limited.[132] Here, the correlation between the cell behavior control and wetting properties is briefly reviewed to show the influence of the surface wettability on the cell response, thus giving clues to control cellular behaviors by altering both the surface wettability and roughness.

A laser-induced silicon spike scaffold with controllable wettability and roughness could serve as a new method to guiding 3D cell−bimaterials interaction in vivo.[133] Many conical microstructures (spikes) at different ratios, dimensions, and densities were achieved by different laser fluences (Figure 9), on which wettability changed from hydrophilic to superhydrophobic and therefore resulted in a disparate fibroblast cell response. Cell adhesion was found to be favored on hydrophilic substrates and inhibited on hydrophobic surfaces, inspired by which a switchable cell-response surface between cell-phobic and cell-philic could be realized by changing a surface to hydrophobic (coating with a hydrophobic silane layer) and hydrophilic (coating with a hydrophilic oxide layer) for the same roughness.

However, not all sorts of cells show the same cellular behavior trend toward hydrophobic surfaces. Through analysis of the effects of material topography and wettability on the cellular proliferation behavior on nonstructured and structured surfaces, it was observed that fibroblast and neuroblastoma reacted differently from hydrophobic surfaces.[134] Neuroblastoma cell proliferation was independent of the surface roughness and hydrophobicity. On the contrary, a reduction tendency of proliferation was observed on a more hydrophobic surface with more roughenss. This could be attributed to the differences in the adhesion mechanism of different cell systems. Fibroblast cells adhered on the surface by means of fibronectin-integrin[135,136] and its whole body.[137] Other adhesion factors

like neuronal cell adhesion molecules served as adhesion receptors, which did not react sensitively to the material hydrophobicity and adhered on surfaces at restrain points in comparison with fibronectin-integrin. Cell specificity was also discovered in human serum albumin (no-cell adhesive) and human plasma fibronectin adsorption on zirconia (MgO-PSZ) bioceramic structured surfaces by CO_2 laser treatment.[138] The albumin adsorption was affected by the surface roughness and wetting characteristics of MgO-PSZ and decreased with these properties, while fibronectin adsorption increased with the wettability characteristics and was predominantly governed by this property.

For a hydrophilic surface, as the surface becomes rougher, the wetting potential becomes higher (i.e., the CA becomes smaller). Modifying the surface properties of 316 LS stainless steel by a CO_2 laser could reduce the CA because of synergic changes in the surface energy and surface roughness.[139] An increase in the wettability of 316 LS stainless steel was observed to be positively related with cell proliferation, which brought about a significant increase in MTT cell proliferation compared with that of the untreated sample. Moreover, a CO_2-laser-treated less CA surface allowed cells not only to adhere and spread better but also to grow faster than either an untreated or a mechanically roughened sample. A similar phenomenon was also observed on a titanium (Ti6Al4V) alloy biometal[140] and MgO-PSZ,[141] on which osteoblast cells adhered and proliferated considerably greater than on the untreated samples. In addition, periodic patterns were also found to be influential to the wettability and osteoblast cell adhesion.[142,143] Ca−P coatings on the Ti6Al4V alloy were separated into spaced line patterns at different intervals. The 100-μm-spaced samples exhibited higher surface energy and increased hydrophilicity compared to untreated Ti6Al4V and 200-μm-spaced samples. Because of increased hydrophilicity in vitro biocompatibility, the samples with 100 μm line spacing gave rise to increased cell proliferation and cell adhesion of mouse MC3T3-E1 osteoblast-like cells.

As mentioned in section 2.4, replication is a fast approach to efficient and effective transfer of hierarchical structures into a biocompatible polymer. The replicas could serve as excellent substrates to tune cellular behaviors.[144] Through replication of laser-induced silicon spikes, negative replicas on PDMS and positive ones on a photocurable (organically modified ceramic) polymer and a biodegradable [poly(lactide-*co*-glycolide)] polymer have been successfully prepared.[145] Cell culture experiments revealed that both fibroblast NIH/3T3 and PC12 neuronal cells showed superior adhesion on micro-replicated polymeric surfaces compared to unstructured ones.

4.4. Wettability Alteration of Dental Hard Tissues. A fs laser technique for modification and structuring of dental hard tissues has emerged as a promising tool because of its many advantages including minimal thermal and mechanical damage, high precision, production of microcrack-free cavities, the absence of a chemical change in treated dental hard tissues, and high processing controllability through spectroscopic feedback.[146−148] Guo et al. found that fs laser treatment could change the wettability of dental hard tissues significantly into superwetting by introducing periodic microgrooves, which would enhance adhesion of restorative materials.[149] Before laser texturing, the CAs of enamel and dentine specimens were 42° and 48°, respectively. After laser treatment, the CAs of both enamel and dentin specimens decreased dramatically to ∼0°. A 1 μL water droplet could rapidly spread on horizontally/vertically settled enamel surface over the laser-treated area (Figure 10). The water spread for a distance of about 4.5 mm is

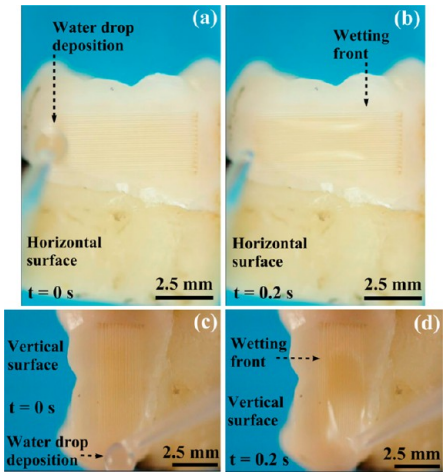

Figure 10. (a and b) Water-spreading dynamics on the laser-treated enamel surface positioned horizontally. (c and d) Water-spreading dynamics on the laser-treated enamel surface positioned vertically.[149] Reproduced with permission from ref 149. Copyright 2011 American Institute Physics.

0.2 s with an average velocity of 22.3 mm/s (Figure 10a,b). Further, the water could sprint vertically uphill against gravity to a distance of 4.3 mm with a spreading velocity of 21.5 mm/s within the first 0.2 s (Figure 10c,d). The pump of liquid uphill was also observed on laser-treated silicon, metal, and glass surfaces.[150,151]

4.5. Paper-Based Devices. Conventional laboratory instruments can provide precise and quantitative analysis of biological samples, but they are inconvenient to be used in emergent situations. What's more, their high cost, the requirement of trained personnel, and considerable volumes of biological samples impede their wide uitilization in less-industrialized countries.[152] Less inexpensive miniature platforms, which are able to do the same bioassays using small volumes,[153] remain a challenge for scientists. Recently, considerable interest has been paid to paper for its low cost, significant flexibility, and tremendous potential to be developed into paper-based devices,[154] such as microfluidic devices[155,156] and sensors.[157,158]

Paper-strip-based assays (dipstick) are one of the most important paper-based devices and have been commercially used for diagnostic tests such as diabetes and pregnancy because of their advantages of ease of use and disposability. They offer an inexpensive platform for colorimetric chemical testing originating from capillary action (e.g., without external pumping) of small-volume fluids. Recently, a platform that could perform a luminol chemiluminescence assay to detect blood was successfully developed.[159] After irradiation of a piece of silicone-coated parchment paper by a CO_2 laser, the original hydrophobic areas transformed into hydrophilic ones with a change in the CA from 115° to 20°. On this hydrophilic−hydrophobic surface, water could only wet the laser-patterned areas, leaving untreated regions completely dry. The modified surfaces exhibited a highly porous structure that could trap/localize chemical and biological aqueous reagents for analysis. A layer of silica microparticles was deposited on the treated areas to cause them to become trapped in porous structures. The

silica particles exhibited excellent adhesion in the porous structures without being taken away by diffusing water or being shaken vigorously. A uniform array of luminol droplets was patterned on the laser-treated surface. The paper platform was carefully placed on a planar surface. Then, blood solution (mice blood diluted in deionized water) was sprayed on the array to mix with luminol droplets at each spot of the array. The catalytic action of iron in the hemoglobin gave rise to chemiluminescence.

4.6. Liquid Separation and Storage. Controlled wettability in different microfluidic channels offers many possibilities for controlling the reagent reaction through control of the liquid medium separation or mixing ratio in different channels. Chang et al. demonstrated the feasibility of an ultrafast laser process to control the wettability on the inner wall surface of microfluidic glass channels.[160] Furthermore, different surface wettabilities have been successfully introduced into each branch of microfluidic channels by fs laser direct ablation of PMMA.[161] By means of changes of various fluences, the original hydrophilic surface (CA ≈ 78°) could change to either hydrophobic (CA ≈ 125°) or superhydrophilic (CA ≈ 0°). A Y-chip made up of two branch channels was designed and fabricated. One channel was written at laser fluences of 5.6 and 1.3 mJ/cm^2, which brought about a hydrophobic (102.5°) or low hydrophilic (64.1°) surface of a channel. The other channel was ablated at a laser fluence of 45.9 mJ/cm^2, resulting in a nearly superhydrophilic surface with CA below 10°. Different water flow velocities were detected for each channel when water was injected into the Y-chip at a flow rate of 1.0 μL/min. The velocity ratio of water flow of the low hydrophilic channel was approximately 3.5 and 9 times that of the highly hydrophilic channel and hydrophobic channel, respectively. The separation velocity and ratio in the two channels could be adjusted by the initial pump rate of the injection syringe.

The laser-achieved "microvessel" surface, which enabled a small volume of aqueous reactants to be kept and analyzed for long periods of time while being protected from evaporation, was reported recently.[162] Fluorinated samples were irradiated in a specific pattern that could take up two different immiscible liquids. Colored water and oil (hexadecane) droplets were placed on the inward and outward concentric circles, respectively. With an increase in the volume of oil by a syringe, the water drop was still trapped in its original position by the outside oil drop. When the outer droplet was touched by a syringe needle, the inner water droplet would float in the "oil chamber" and disaffiliate from the patterned structure. Using a similar method, it is possibile to add or extract aqueous reactants from the oil droplet.

5. CONCLUSIONS AND FUTURE PERSPECTIVES

Nature has been a source of inspiration for the development of artificial surfaces with novel properties and unique functions. Significant progress has been made in the realization of a wide variety of bioinspired wettabilities through various techniques. As a noncontact, maskless, low-cost technique, laser microfabrication has already been demonstrated as an exciting platform to develop controllable wettability on different materials. Four relative laser processing techniques, including laser direct writing, PLD, laser textured templating, and laser IL, can establish a large variety of structures ranging from single scale (nano- or microscale) to multiscale (including both micro- and nanoscale). In particular, compared to other techniques, two unique characteristics guarantee their future prosperity. The first one is the ability to tune the surface wettability from superhydrophilic to superhydrophobic without the need for fluorination, which can be extensively applied in the manipulation of cellular behaviors. The second one is the natural introduction of nanoroughness during the ablation process, which facilitates the generation of hierarchical dual-scale structures in favor of superhydrophobicity. The structures achieved by laser processing have recently been widely applied in various fields, such as smart stimuli-responsive switchable surfaces, paper-based devices, controllable biocompatible surfaces, and microfluidic devices, all of which are direct impetuses impelling the field to move forward rapidly.

Laser processing for the development of various wettabilities is in its infancy and still faces many problems that must be addressed for further study. First and foremost, the underlying mechanism that is responsible for the formation of micro- and nanostructures is still unclear. Relationships between the morphology, density, and size of multiscale structures and the processing laser parameters, such as laser fluence, scanning speed, polarization, and environment (air, vacuum, and O_2), are still under discussion, upon which a scientist could precisely tune the structure according to the need for different conditions. The second issue is the processing speed and throughput. The scanning speed of laser processing, especially for laser direct writing, is low because of its nature of being series processing. It is expected that alternative approaches will be explored on the basis of laser microfabrication, which can greatly improve the processing efficiency. Cooperation of the laser technique with the chemical etching technique and nanoimprint has been successfully used to develop microlens arrays with different sizes and layout.[163−168] The synthetic effect of these three techniques can give rise to large area structures in only several hours, far faster than laser direct writing. Another strategy is to realize parallel processing by means of DOE, which can split a single incident beam into hundreds to thousands of tiny "light pens" and etch a large area in one process step.[169] In addition, whether a laser can produce more artificial bioinspired surfaces that mimic both the structures and functions, whether laser-achieve wetting surfaces can respond to more external stimuli, such as acid, magnetic, and light, whether laser processing can realize more intelligent wettability modulation, and how various wettabilities can be applied in microfluidic devices are still necessary to make further investigations. These will be beneficial for the wide use of a laser in the fabrication of more advanced integrated multifunctional materials in real life.

AUTHOR INFORMATION

Corresponding Author

*E-mail: chenfeng@mail.xjtu.edu.cn.

Notes

The authors declare no competing financial interest.

ACKNOWLEDGMENTS

This work is surported by the National Science Foundation of China under Grants 61275008 and 61176113, the special-funded programme on national key scientific instruments and equipment development of China under Grant 2012YQ12004706, and the Fundamental Research Funds for the Central Universities.

REFERENCES

(1) Koch, K.; Bhushan, B.; Barthlott, W. *Prog. Mater. Sci.* **2009**, *54*, 137−178.
(2) Xia, F.; Jiang, L. *Adv. Mater.* **2008**, *20*, 2842−2858.
(3) Sun, T. L.; Qing, G. Y.; Su, B. L.; Jiang, L. *Chem. Soc. Rev.* **2011**, *40*, 2909−2921.
(4) Yao, X.; Song, Y.; Jiang, L. *Adv. Mater.* **2011**, *23*, 719−734.
(5) Sun, T. L.; Qing, G. Y. *Adv. Mater.* **2011**, *23*, H57−H77.
(6) Barthlott, W.; Neinhuis, C. *Planta* **1997**, *202*, 1−8.
(7) Barthlott, W.; Schimmel, T.; Wiersch, S.; Koch, K.; Brede, M.; Barczewski, M.; Walheim, S.; Weis, A. *Adv. Mater.* **2010**, *22*, 2325−2328.
(8) Gao, X. F.; Yan, X.; Yao, X.; Xu, L.; Zhang, K.; Zhang, J. H.; Yang, B.; Jiang, L. *Adv. Mater.* **2007**, *19*, 2213−2217.
(9) Xia, F.; Jiang, L. *Adv. Mater.* **2008**, *20*, 2842−2858.
(10) Hansen, W. R.; Autumn, K. *Proc. Natl. Acad. Sci. U. S. A.* **2005**, *102*, 385−389.
(11) Parker, A. R.; Lawrence, C. R. *Nature* **2001**, *414*, 33−34.
(12) Yan, Y. Y.; Gao, N.; Barthlott, W. *Adv. Colloid Interface Sci.* **2011**, *169*, 80−105.
(13) Hare, E. F.; Shafrin, E. G.; Zisman, W. A. *J. Phys. Chem.* **1954**, *58*, 236−239.
(14) Li, X. M.; Reihoudt, D.; Crego-Calama, M. *Chem. Soc. Rev.* **2007**, *36*, 1350−1368.
(15) Stratakis, E.; Ranella, A.; Farsari, M.; Fotakis, C. *Prog. Quantum Electron.* **2009**, *33*, 127−163.
(16) Lau, K. S.; Chan, P. W.; Wong, K. H.; Yeung, K. W.; Chan, K.; Gong, W. Z. *J. Mater. Process. Technol.* **1997**, *63*, 524−528.
(17) Lawrence, J.; Li, L. *Opt. Laser Eng.* **2000**, *32*, 353−365.
(18) Anastasiadis, S. H. *Langmuir* **2013**, DOI: dx.doi.org/10.1021/la400533u.
(19) Hao, L.; Lawrence, J.; Li, L. *Surf. Coat. Technol.* **1999**, *115*, 273−281.
(20) Lawrence, J.; Li, L. *Mater. Sci. Eng., A* **2001**, *303*, 142−149.
(21) Hao, L.; Lawrence, J.; Li, L. *Appl. Surf. Sci.* **2005**, *247*, 453−457.
(22) Chichkov, B. N.; Momma, C.; Nolte, S.; Von Alvensleben, F.; Tünnermann, A. *Appl. Phys. A: Mater. Sci. Process.* **1996**, *63*, 109−115.
(23) Momma, C.; Nolte, S.; Chichkov, B. N.; Alvensleben, F. V.; Tünnermann, A. *Appl. Surf. Sci.* **1997**, *109/110*, 15−19.
(24) Chen, F.; Zhang, D. S.; Yang, Q.; Wang, X. H.; Dai, B. J.; Li, X. M.; Hao, X. Q.; Ding, Y. C.; Si, J. H. *Langmuir* **2011**, *27*, 359−365.
(25) Shen, M. Y.; Crouch, C. H.; Carey, J. E.; Mazur, E. *Appl. Phys. Lett.* **2004**, *85*, 5694−5696.
(26) Shen, M.; Carey, J. E.; Crouch, C. H.; Kandyla, M.; Stone, H. A.; Mazur, E. *Nano Lett.* **2008**, *8*, 2087−2091.
(27) Varlamova, O.; Costache, F.; Ratzke, M.; Reif, J. *Appl. Surf. Sci.* **2007**, *253*, 7932−7936.
(28) Vorobyev, A. Y.; Guo, C. L. *Appl. Surf. Sci.* **2007**, *253*, 7272−7280.
(29) Birnbaum, M. *J. Appl. Phys.* **1965**, *36*, 3688.
(30) Huang, M.; Zhao, F. L.; Cheng, Y.; Xu, N. S.; Xu, Z. Z. *ACS Nano* **2009**, *3*, 4062−4070.
(31) Zhao, Q. Z.; Malzer, S.; Wang, L. J. *Opt. Express* **2007**, *15*, 15741−15746.
(32) Le Harzic, R.; Dörr, D.; Sauer, D.; Neumeier, M.; Epple, M.; Zimmermann, H.; Stracke, F. *Opt. Lett.* **2011**, *36*, 229−231.
(33) Wu, B.; Zhou, M.; Li, J.; Ye, X.; Li, G.; Cai, L. *Appl. Surf. Sci.* **2009**, *256*, 61−66.
(34) Bonse, J.; Wrobel, J. M.; Krüger, J.; Kautek, W. *Appl. Phys. A: Mater. Sci. Process.* **2001**, *72*, 89−94.
(35) Bonse, J.; Baudach, S.; Krüger, J.; Kautek, W.; Lenzner, M. *Appl. Phys. A: Mater. Sci. Process.* **2002**, *74*, 19−25.
(36) Oliveira, V.; Ausset, S.; Vilar, R. *Appl. Surf. Sci.* **2009**, *255*, 7556−7560.
(37) Jagdheesh, R.; Pathiraj, B.; Karatay, E.; Römer, G. R. B. E.; Huis in't Veld, A. J. *Langmuir* **2011**, *27*, 8464−8469.
(38) Wong, W.; Chan, K.; Yeung, K. W.; Lau, K. S. *J. Mater. Process. Technol.* **2003**, *132*, 114−118.
(39) Baldacchini, T.; Carey, J. E.; Zhou, M.; Mazur, E. *Langmuir* **2006**, *22*, 4917−4919.
(40) Crouch, C. H.; Carey, J. E.; Warrender, J. M.; Aziz, M. J.; Mazur, E.; Génin, F. Y. *Appl. Phys. Lett.* **2004**, *84*, 1850−1852.
(41) Zhao, H.; Law, K. Y.; Sambhy, V. *Langmuir* **2011**, *27*, 5927−5935.
(42) Zorba, V.; Stratakis, E.; Barberoglou, M.; Spanakis, E.; Tzanetakis, P.; Fotakis, C. *Appl. Phys. A: Mater. Sci. Process.* **2008**, *93*, 819−825.
(43) Barberoglou, M.; Zorba, V.; Stratakis, E.; Spanakis, E.; Tzanetakis, P.; Anastasiadis, S. H.; Fotakis, C. *Appl. Surf. Sci.* **2009**, *255*, 5425−5429.
(44) Gao, X. F.; Yao, X.; Jiang, L. *Langmuir* **2007**, *23*, 4886−4891.
(45) Zhou, M.; Yang, H. F.; Li, B. J.; Dai, J.; Di, J. K.; Zhao, E. L.; Cai, L. *Appl. Phys. A: Mater. Sci. Process.* **2009**, *94*, 571−576.
(46) Tiaw, K. S.; Goh, S. W.; Hong, M.; Wang, Z.; Lanb, B.; Teoh, S. H. *Biomaterials* **2005**, *26*, 763−769.
(47) De Marco, C.; Eaton, S. M.; Suriano, R.; Turri, S.; Levi, M.; Ramponi, R.; Cerullo, G.; Osellame, R. *ACS Appl. Mater. Interfaces* **2010**, *2*, 2377−2384.
(48) Wang, Z. K.; Zheng, H. Y.; Lim, C. P.; Lam, Y. C. *Appl. Phys. Lett.* **2009**, *95*, 111110.
(49) Qi, H.; Chen, T.; Yao, L. Y.; Zuo, T. C. *Microfluid. Nanofluid.* **2008**, *5*, 139−143.
(50) Dahotre, N. B.; Paital, S. R.; Samant, A. N.; Daniel, C. *Philos. Trans. R. Soc., A* **2010**, *368*, 1863−1889.
(51) Paital, S. R.; Dahotre, N. B. *Acta Biomater.* **2009**, *5*, 2763−2772.
(52) Cassie, B. D.; Baxter, S. *Trans. Faraday Soc.* **1944**, *40*, 546−551.
(53) Feng, X. J.; Jiang, L. *Adv. Mater.* **2006**, *18*, 3063−3078.
(54) Gao, L.; McCarthy, T. J. *Langmuir* **2006**, *22*, 2966−2967.
(55) Feng, L.; Li, S.; Li, Y.; Li, H.; Zhang, L.; Zhai, J.; Song, Y.; Liu, B.; Jiang, L.; Zhu, D. *Adv. Mater.* **2002**, *14*, 1857−1860.
(56) Wang, S.; Jiang, L. *Adv. Mater.* **2007**, *19*, 3423−3424.
(57) Wang, X. H.; Chen, F.; Liu, H. W.; Liang, W. W.; Yang, Q.; Si, J. H.; Hou, X. *Appl. Surf. Sci.* **2009**, *255*, 8483−8487.
(58) Misawa, H.; Kondo, T.; Juodkazis, S.; Mizeikis, V.; Matsuo, S. *Opt. Express* **2006**, *14*, 7943−7953.
(59) Xia, D.; Ku, Z.; Lee, S. C.; Brueck, S. R. J. *Adv. Mater.* **2011**, *23*, 147−179.
(60) Jang, J. H.; Ullal, C. K.; Maldovan, M.; Gorishnyy, T.; Kooi, S.; Koh, C.; Thomas, E. L. *Adv. Funct. Mater.* **2007**, *17*, 3027−3041.
(61) Zhao, Y.; Lu, Q. H.; Li, M.; Li, X. *Langmuir* **2007**, *23*, 6212−6217.
(62) Wu, S. Z.; Wu, D.; Yao, J.; Chen, Q. D.; Wang, J. N.; Niu, L. G.; Fang, H. H.; Sun, H. B. *Langmuir* **2010**, *26*, 12012−12016.
(63) Xia, D.; He, X.; Jiang, Y. B.; Lopez, G. P.; Brueck, S. R. J. *Langmuir* **2010**, *26*, 2700−2706.
(64) Xia, D.; Brueck, S. R. J. *Nano Lett.* **2008**, *8*, 2819−2824.
(65) Yang, Y. L.; Hsu, C. C.; Chang, T. L.; Kuo, L. S.; Chen, P. H. *Appl. Surf. Sci.* **2010**, *256*, 3683−3687.
(66) Wu, D.; Wu, S. Z.; Chen, Q. D.; Zhao, S.; Zhang, H.; Jiao, J.; Piersol, J. A.; Wang, J. N.; Sun, H. B.; Jiang, L. *Lab Chip* **2011**, *11*, 3873−3879.
(67) Wu, D.; Chen, Q. D.; Xia, H.; Jiao, J.; Xu, B. B.; Lin, X. F.; Xu, Y.; Sun, H. B. *Soft Matter* **2010**, *6*, 263−267.
(68) Patel, N.; Fernandes, R.; Guella, G.; Kale, A.; Miotello, A.; Patton, B.; Zanchetta, C. *J. Phys. Chem. C* **2008**, *112*, 6968−6976.
(69) Lardé, R.; Talbot, E.; Pareige, P.; Bieber, H.; Schmerber, G.; Colis, S.; Pierron-Bohnes, V.; Dinia, A. *J. Am. Chem. Soc.* **2011**, *133*, 1451−1458.
(70) Schou, J. *Appl. Surf. Sci.* **2009**, *255*, 5191−5198.
(71) Daoud, W. A.; Xin, J. H.; Zhang, Y. H.; Mak, C. L. *Thin Solid Films* **2006**, *515*, 835−837.
(72) Kwong, H. Y.; Wong, M. H.; Wong, Y. W.; Wong, K. H. *Appl. Surf. Sci.* **2007**, *253*, 8841−8845.
(73) Li, L.; Li, Y.; Gao, S.; Koshizaki, N. *J. Mater. Chem.* **2009**, *19*, 8366−8371.
(74) Li, Y.; Sasaki, T.; Shimizu, Y.; Koshizaki, N. *Small* **2008**, *4*, 2286−2291.

(75) Li, L.; Koshizaki, N. *J. Mater. Chem.* **2010**, *20*, 2972−2978.
(76) Li, Y.; Sasaki, T.; Shimizu, Y.; Koshizaki, N. *J. Am. Chem. Soc.* **2008**, *130*, 14755−14762.
(77) Duffy, D. C.; McDonald, J. C.; Schueller, O. J. A.; Whitesides, G. M. *Anal. Chem.* **1998**, *70*, 4974−4984.
(78) Abate, A. R.; Krummel, A. T.; Lee, D.; Marquez, M.; Holtze, C.; Weitz, D. A. *Lab Chip* **2008**, *8*, 2157−2160.
(79) Wang, X. C.; Wu, L. Y. L.; Shao, Q.; Zheng, H. Y. *J. Micromech. Microeng.* **2009**, *19*, 085025.
(80) Wu, L. Y. L.; Shao, Q.; Wang, X. C.; Zheng, H. Y.; Wong, C. C. *Soft Matter* **2012**, *8*, 6232−6238.
(81) Wu, P. H.; Cheng, C. W.; Chang, C. P.; Wu, T. M.; Wang, J. K. *J. Micromech. Microeng.* **2011**, *21*, 115032.
(82) Sarrat, B.; Pécheyran, C.; Bourrigaud, S.; Billon, L. *Langmuir* **2011**, *27*, 3174−3179.
(83) De Marco, C.; Eaton, S. M.; Levi, M.; Cerullo, G.; Turri, S.; Osellame, R. *Langmuir* **2011**, *27*, 8391−8395.
(84) Yoon, T. O.; Shin, H. J.; Jeoung, S. C.; Park, Y. *Opt. Express* **2008**, *16*, 12715−12725.
(85) Dawood, M. K.; Zheng, H.; Liew, T. H.; Leong, K. C.; Foo, Y. L.; Rajagopalan, R.; Khan, S. A.; Choi, W. K. *Langmuir* **2011**, *27*, 4126−4133.
(86) Jokinen, V.; Sainiemi, L.; Franssila, S. *Adv. Mater.* **2008**, *20*, 3453−3456.
(87) Pfleging, W.; Kohler, R.; Torge, M.; Trouillet, V.; Danneil, F.; Stüber, M. *Appl. Surf. Sci.* **2011**, *257*, 7907−7912.
(88) Zorba, V.; Persano, L.; Pisignano, D.; Athanassiou, A.; Stratakis, E.; Cingolani, R.; Tzanetakis, P.; Fotakis, C. *Nanotechnology* **2006**, *17*, 3234−3238.
(89) Bizi-Bandoki, P.; Benayoun, S.; Valette, S.; Beaugiraud, B.; Audouard, E. *Appl. Surf. Sci.* **2011**, *257*, 5213−5218.
(90) Luo, B. H.; Shum, P. W.; Zhou, Z. F.; Li, K. Y. *Surf. Coat. Technol.* **2010**, *204*, 1180−1185.
(91) He, L.; Chen, J.; Farson, D. F.; Lannutti, J. J.; Rokhlin, S. I. *Appl. Surf. Sci.* **2011**, *257*, 3547−3553.
(92) Nunes, B.; Serro, A. P.; Oliveira, V.; Montemor, M. F.; Alves, E.; Saramago, B.; Colço, R. *Appl. Surf. Sci.* **2011**, *257*, 2604−2609.
(93) Pfleging, W.; Bruns, M.; Welle, A.; Wilson, S. *Appl. Surf. Sci.* **2007**, *253*, 9177−9184.
(94) Pfleging, W.; Torge, M.; Bruns, M.; Trouillet, V.; Welle, A.; Wilson, S. *Appl. Surf. Sci.* **2009**, *255*, 5453−5457.
(95) Rossier, J. S.; Bercier, P.; Schwarz, A.; Loridant, S.; Girault, H. H. *Langmuir* **1999**, *15*, 5173−5178.
(96) Kietzig, A. M.; Hatzikiriakos, S. G.; Englezos, P. *Langmuir* **2009**, *25*, 4821−4827.
(97) Zhao, Y.; Xie, S.; Jiang, Y. *Surf. Interface Anal.* **2012**, *44*, 1360−1363.
(98) Kam, D. H.; Bhattacharya, S.; Mazumder, J. *J. Micromech. Microeng.* **2012**, *22*, 105019.
(99) Bhushan, B.; Jung, Y. C.; Koch, K. *Philos. Trans. R. Soc., A* **2009**, *367*, 1631−1672.
(100) Lee, S. M.; Jung, I. D.; Ko, J. S. *J. Micromech. Microeng.* **2008**, *18*, 125007.
(101) Park, H. K.; Yoon, S. W.; Do, Y. R. *J. Mater. Chem.* **2012**, *22*, 14035−14041.
(102) Matsumura, T.; Kazama, A.; Yagi, T. *Appl. Phys. A: Mater. Sci. Process.* **2005**, *81*, 1393−1398.
(103) Wagterveld, R. M.; Berendsen, C. W. J.; Bouaidat, S.; Jonsmann, J. *Langmuir* **2006**, *22*, 10904−10908.
(104) Xia, F.; Zhu, Y.; Feng, L.; Jiang, L. *Soft Matter* **2009**, *5*, 275−281.
(105) Xin, B.; Hao, J. *Chem. Soc. Rev.* **2010**, *39*, 769−782.
(106) Barberoglou, M.; Zorba, V.; Pagozidis, A.; Fotakis, C.; Stratakis, E. *Langmuir* **2010**, *26*, 13007−13014.
(107) Papadopoulou, E. L.; Zorba, V.; Pagkozidis, A.; Barberoglou, M.; Stratakis, E.; Fotakis, C. *Thin Solid Films* **2009**, *518*, 1267−1270.
(108) Papadopoulou, E. L.; Barberoglou, M.; Zorba, V.; Manousaki, A.; Pagkozidis, A.; Stratakis, E.; Fotakis, C. *J. Phys. Chem. C* **2009**, *113*, 2891−2895.
(109) Athanassiou, A.; Lygeraki, M. I.; Pisignano, D.; Lakiotaki, K.; Varda, M.; Mele, E.; Fotakis, C.; Cingolani, R.; Anastasiadis, S. H. *Langmuir* **2006**, *22*, 2329−2333.
(110) Sun, T.; Wang, G.; Feng, L.; Liu, B.; Ma, Y.; Jiang, L.; Zhu, D. *Angew. Chem., Int. Ed.* **2004**, *43*, 357−360.
(111) Zhang, D. S.; Chen, F.; Yang, Q.; Si, J. H.; Hou, X. *Soft Matter* **2011**, *7*, 8337−8342.
(112) Zhang, X. Y.; Mi, Y. L. *Langmuir* **2009**, *25*, 3212−3218.
(113) Wu, D.; Wu, S. Z.; Chen, Q. D.; Zhang, Y. L.; Yao, J.; Yao, X.; Niu, L. G.; Wang, J. N.; Jiang, L.; Sun, H. B. *Adv. Mater.* **2011**, *23*, 545−549.
(114) Ma, M.; Hill, R. M. *Curr. Opin. Colloid Interface Sci.* **2006**, *11*, 193−202.
(115) Zorba, V.; Stratakis, E.; Barberoglou, M.; Spanakis, E.; Tzanetakis, P.; Anastasiadis, S. H.; Fotakis, C. *Adv. Mater.* **2008**, *20*, 4049−4054.
(116) Feng, L.; Zhang, Y. A.; Xi, J. M.; Zhu, Y.; Wang, N.; Xia, F.; Jiang, L. *Langmuir* **2008**, *24*, 4114−4119.
(117) Wang, J. N.; Shao, R. Q.; Zhang, Y. L.; Guo, L.; Jiang, H. B.; Lu, D. X.; Sun, H. B. *Chem.—Asian J.* **2012**, *7*, 301−304.
(118) Zhang, Y. L.; Jin, Z.; Kim, E.; Sun, H. B. *Nanoscale* **2012**, *4*, 4858−4869.
(119) Zhang, D. S.; Chen, F.; Fang, G. P.; Yang, Q.; Xie, D. G.; Qiao, G. J.; Li, W.; Si, J. H.; Hou, X. *J. Micromech. Microeng.* **2010**, *20*, 075029.
(120) Zhang, D. S.; Chen, F.; Yang, Q.; Yong, J. L.; Bian, H.; Ou, Y.; Si, J. H.; Meng, X. W.; Hou, X. *ACS Appl. Mater. Interfaces* **2012**, *4*, 4905−4912.
(121) Gao, J.; Liu, Y.; Xu, H.; Wang, Z.; Zhang, X. *Langmuir* **2009**, *25*, 4365−4369.
(122) Gao, J.; Liu, Y.; Xu, H.; Wang, Z.; Zhang, X. *Langmuir* **2010**, *26*, 9673−9676.
(123) Curtis, A.; Wilkinson, C. *Biomaterials* **1997**, *18*, 1573−1583.
(124) Flemming, R. G.; Murphy, C. J.; Abrams, Z. A.; Goodman, S. L.; Nealey, P. F. *Biomaterials* **1999**, *20*, 573−588.
(125) Lord, M. S.; Foss, M.; Besenbacher, F. *Nano Today* **2010**, *5*, 66−78.
(126) Geyer, F. L.; Ueda, E.; Liebel, U.; Grau, N.; Levkin, P. A. *Angew. Chem., Int. Ed.* **2011**, *50*, 8424−8427.
(127) Yohe, S. T.; Colson, Y. L.; Grinstaff, M. W. *J. Am. Chem. Soc.* **2012**, *134*, 2016−2019.
(128) Piret, G.; Galopin, E.; Coffinier, Y.; Boukherroub, R.; Legrand, D.; Slomianny, C. *Soft Matter* **2011**, *7*, 8642−8649.
(129) Stratakis, E.; Ranella, A.; Farsari, M.; Fotakis, C. *Prog. Quant. Electron.* **2009**, *33*, 127−163.
(130) Lee, B. L. P.; Jeon, H.; Wang, A.; Yan, Z.; Yu, J.; Grigoropoulos, C. P. *Acta Biomater.* **2012**, *8*, 2648−2658.
(131) Jeon, H.; Hidai, H.; Hwang, D. J.; Healy, K. E.; Grigoropoulos, C. P. *Biomaterials* **2010**, *31*, 4286−4295.
(132) Schlie, S.; Fadeeva, E.; Koroleva, A.; Ovsianikov, A.; Koch, J.; Ngezahayo, A.; Chichkov, B. N. *Photonics Nanostruct.* **2011**, *9*, 159−162.
(133) Ranella, A.; Barberoglou, M.; Bakogianni, S.; Fotakis, C.; Stratakis, E. *Acta Biomater.* **2010**, *6*, 2711−2720.
(134) Fadeeva, E.; Schlie, S.; Koch, J.; Ngezahayo, A.; Chichkov, B. N. *Phys. Status Solidi A* **2009**, *206*, 1348−1351.
(135) Meadows, P. Y.; Walker, G. C. *Langmuir* **2005**, *21*, 4096−4107.
(136) García, A. J.; Vega, M. D.; Boettiger, D. *Mol. Biol.* **1999**, *10*, 785−798.
(137) Schlie, S.; Fadeeva, E.; Koch, J.; Ngezahayo, A.; Chichkov, B. N. *J. Biomater. Appl.* **2009**, *25*, 217−233.
(138) Hao, L.; Lawrence, J. *J. Biomed. Mater. Res. A* **2004**, *69*, 748−756.
(139) Hao, L.; Lawrence, J.; Phua, Y. F.; Chian, K. S.; Lim, G. C.; Zheng, H. Y. *J. Biomed. Mater. Res. B* **2005**, *73*, 148−156.
(140) Hao, L.; Lawrence, J. *Surf. Coat. Technol.* **2006**, *200*, 5581−5589.
(141) Hao, L.; Lawrence, J. *Mater. Sci. Eng., C* **2003**, *23*, 627−639.

(142) Paital, S. R.; He, W.; Dahotre, N. B. *J. Mater. Sci.: Mater. Med.* **2010**, *21*, 2187−2200.
(143) Paital, S. R.; Cao, Z.; He, W.; Dahotre, N. B. *Biofabrication* **2010**, *2*, 025001.
(144) Pernites, R. B.; Santos, C. M.; Maldonado, M.; Ponnapati, R. R.; Rodrigues, D. F.; Advincula, R. C. *Chem. Mater.* **2012**, *24*, 870−880.
(145) Koufaki, N.; Ranella, A.; Aifantis, K. E.; Barberoglou, M.; Psycharakis, S.; Fotakis, C.; Stratakis, E. *Biofabrication* **2011**, *3*, 045004.
(146) Niemz, M. H.; Kasenbacher, A.; Strassl, M.; Bäcker, A.; Beyertt, A.; Nickel, D.; Giesen, A. *Appl. Phys. B: Lasers Opt.* **2004**, *79*, 269−271.
(147) Daskalova, A.; Bashir, S.; Husinsky, W. *Appl. Surf. Sci.* **2010**, *257*, 1119−1124.
(148) Krüger, J.; Kautek, W.; Newesely, H. *Appl. Phys. A: Mater. Sci. Process.* **1999**, *69*, S403−S407.
(149) Vorobyev, A. Y.; Guo, C. L. *Appl. Phys. Let.* **2011**, *99*, 193703.
(150) Vorobyev, Y.; Guo, C. L. *Opt. Express* **2010**, *18*, 6455−6460.
(151) Vorobyev, Y.; Guo, C. L. *Appl. Phys. Lett.* **2009**, *94*, 224102.
(152) Mabey, D.; Peeling, R. W.; Ustianowski, A.; Perkins, M. D. *Nat. Rev. Microbiol.* **2004**, *2*, 231−240.
(153) Chin, C. D.; Laksanasopin, T.; Cheung, Y. K.; Steinmiller, D.; Linder, V.; Parsa, H.; Wang, J.; Moore, H.; Rouse, R.; Umviligihozo, G.; Karita, E.; Mwambarangwe, L.; Braunstein, S. L.; Wijgert, J.; Sahabo, R.; Justman, J. E.; El-Sadr, W.; Sia, S. K. *Nat. Med.* **2011**, *17*, 1015−1019.
(154) Martinez, A. W.; Phillips, S. T.; Butte, M. J.; Whitesides, G. M. *Angew. Chem., Int. Ed.* **2007**, *46*, 1318−1320.
(155) Martinez, A. W.; Phillips, S. T.; Wiley, B. J.; Gupta, M.; Whitesides, G. M. *Lab Chip* **2008**, *8*, 2146−2150.
(156) Martinez, A. W.; Phillips, S. T.; Whitesides, G. M. *Anal. Chem.* **2010**, *82*, 3−10.
(157) Struss, A.; Pasini, P.; Ensor, C. M.; Raut, N.; Daunert, S. *Anal. Chem.* **2010**, *82*, 4457−4463.
(158) Parolo, C.; Merkoçi, A. *Chem. Soc. Rev.* **2013**, *42*, 450−457.
(159) Chitnis, G.; Ding, Z.; Chang, C. L.; Savranacde, C. A.; Ziaie, B. *Lab Chip* **2011**, *11*, 1161−1165.
(160) Chang, T. L.; Tsai, T. K.; Yang, H. P.; Huang, J. Z. *Microelectron. Eng.* **2012**, *98*, 684−688.
(161) Wang, Z. K.; Zheng, H. Y.; Xia, H. M. *Microfluid. Nanofluid.* **2011**, *10*, 225−229.
(162) Stojanovic, A.; Artus, G. R. J.; Seeger, S. *Nano Res.* **2010**, *3*, 889−894.
(163) Chen, F.; Liu, H. W.; Yang, Q.; Wang, X. H.; Hou, C.; Bian, H.; Liang, W. W.; Si, J. H.; Hou, X. *Opt. Express* **2010**, *18*, 20334−20343.
(164) Qu, P. B.; Chen, F.; Liu, H. W.; Yang, Q.; Lu, J.; Si, J. H.; Wang, Y. Q.; Hou, X. *Opt. Express* **2012**, *20*, 5775−5782.
(165) Hao, B.; Liu, H. W.; Chen, F.; Yang, Q.; Qu, P. B.; Du, G. Q.; Si, J. H.; Wang, X. H.; Hou, X. *Opt. Express* **2012**, *20*, 12939−12948.
(166) Liu, H. W.; Chen, F.; Yang, Q.; Qu, P. B.; Si, J. H.; Hou, X. *Appl. Phys. Lett.* **2012**, *100*, 133701.
(167) Du, G. Q.; Yang, Q.; Chen, F.; Liu, H. W.; Deng, Z. F.; Bian, H.; He, S. G.; Si, J. H.; Meng, X. W.; Hou, X. *Opt. Lett.* **2012**, *37*, 4404.
(168) Deng, Z. F.; Chen, F.; Yang, Q.; Liu, H. W.; Bian, H.; Du, G. Q.; Hu, Y.; Si, J. H.; Meng, X. W.; Hou, X. *J. Micromech. Microeng.* **2012**, *22*, 115026.
(169) Bekesi, J.; Kaakkunen, J. J. J.; Michaeli, W.; Klaiber, F.; Schoengart, M.; Ihlemann, J.; Simon, P. *Appl. Phys. A: Mater. Sci. Process.* **2010**, *99*, 691−695.